

Article

Fortifying Slab Resilience against Touch-Off Explosions: Integration of Innovative Stud Reinforcements and Computational Analysis

S. M. Anas ^{1,*} , Rayeh Nasr Al-Dala'ien ^{2,3} , Mohd Shariq ¹  and Mehtab Alam ⁴

¹ Department of Civil Engineering, Jamia Millia Islamia (A Central University), New Delhi 110025, India; shariqq786@gmail.com

² Civil Engineering Department, College of Engineering, Al-Balqa Applied University (BAU), Salt 19117, Jordan; rayah.nasr1@bau.edu.jo

³ College of Graduate Studies, Universiti Tenaga Nasional, Jalan Ikram-UNITEN, Kajang 43000, Malaysia

⁴ Department of Civil Engineering, Netaji Subhas University of Technology, New Delhi 110073, India; mehtab.alam@nsut.ac.in

* Correspondence: s1910521@st.jmi.ac.in

Abstract: Explosions, once limited to military and accidental contexts, now occur frequently due to advances in warfare, local disputes, and global conflicts. Recent incidents, like urban bombings, emphasize the urgent need for infrastructure to withstand explosions. Slabs, critical in architectural frameworks, are vulnerable to explosive forces due to their slimness, making them prime targets for sabotage. Scholars have explored various strategies to fortify slabs, including the use of advanced materials like CFRP laminates/strips, steel sheets and ultra-high-strength concrete, along with reinforcement techniques such as two-mesh and diagonal reinforcements. A novel approach introduced in current research involves integrating vertical short bars, or studs, to enhance slab resilience against touch-off explosions. The aim of this research endeavor is to assess the impact of studs and their utilization in bolstering the anti-contact-blast capabilities of a concrete slab. To achieve this goal, a specialized framework within the ABAQUS/Explicit 2020 software is employed for comprehensive analysis. Initially, a conventionally reinforced slab devoid of studs serves as the benchmark model for numerical validation, facilitating a comparative assessment of its anti-contact-blast effectiveness against the findings outlined by Zhao and colleagues in 2019. Following successful validation, six additional distinct slab models are formulated utilizing sophisticated software, incorporating studs of varying heights, namely, 15 mm and 10 mm. Each configuration encompasses three distinct welding scenarios: (i) integration with upper-layer bars, (ii) attachment to bottom-layer bars, and (iii) connection to both upper- and bottom-layer bars. The comparative merits of the slabs are evaluated and deliberated upon through the examination of diverse response parameters. The research revealed that the incorporation of studs within slabs yielded notable enhancements in blast resistance. Specifically, taller studs demonstrated exceptional resilience against deformation, cracking, and perforation, while also diminishing plastic damage energy. Particularly noteworthy was the superior performance observed in slabs with studs welded to both upper and lower layers of re-bars. This highlights the critical significance of both the integration of studs and their precise positioning in fortifying structural integrity against blast-induced loadings.

Keywords: blast mitigation; explosions; infrastructure resilience; reinforcement techniques; slab vulnerability; stud integration



Citation: Anas, S.M.; Al-Dala'ien, R.N.; Shariq, M.; Alam, M. Fortifying Slab Resilience against Touch-Off Explosions: Integration of Innovative Stud Reinforcements and Computational Analysis. *Buildings* **2024**, *14*, 1468. <https://doi.org/10.3390/buildings14051468>

Academic Editor: Yonghui Wang

Received: 17 April 2024

Revised: 2 May 2024

Accepted: 16 May 2024

Published: 18 May 2024



Copyright: © 2024 by the authors. Licensee MDPI, Basel, Switzerland. This article is an open access article distributed under the terms and conditions of the Creative Commons Attribution (CC BY) license (<https://creativecommons.org/licenses/by/4.0/>).

1. Introduction

Explosions, characterized by abrupt and forceful releases of energy, have witnessed a notable escalation in prevalence across diverse contexts in recent times [1–3]. Touch-off

explosions [2,3], a distinct category within the spectrum of explosive events, entail positioning the explosive device in direct physical contact with the intended target. Instances of touch-off explosions encompass parcel bombs, suitcase bombs, and analogous contrivances meticulously engineered to induce swift and confined devastation upon activation. From the complexities of modern warfare to localized conflicts and geopolitical tensions, the incidence of explosions has surged, presenting formidable risks to both human life and critical infrastructure [2–5]. In contemporary warfare, advancements in technology have facilitated the development of increasingly sophisticated explosive devices, resulting in catastrophic ramifications on battlefields worldwide. Moreover, political instability and regional disputes have erupted into armed confrontations, frequently culminating in explosions within civilian domains. Furthermore, terrorist factions and extremist entities have strategically employed explosives as primary instruments of harm, targeting densely populated public areas and vital infrastructure installations [5]. Recent events, including bombings in urban centers, assaults on transportation systems, and industrial mishaps, underscore the imperative for heightened measures to mitigate the impact of explosions. There exists a compelling urgency to fortify infrastructure and facilities against explosive threats to a certain threshold, employing state-of-the-art materials, innovative structural configurations, and robust security protocols to safeguard lives and uphold the resilience of essential services amid evolving adversities.

Slabs within architectural frameworks serve as pivotal horizontal structural constituents, underpinning floors, roofs, and ceilings, while orchestrating the distribution of loads to ensure structural steadfastness [4–6]. Despite their indispensable role, slabs, owing to their inherently slim and pliant characteristics, are markedly susceptible to the abrupt and intense strain rates induced by explosive forces. Contact blasts, exemplified by parcel bombs or suitcase explosives, exhibit a straightforward yet exceedingly efficacious method of sabotage when directed specifically at slabs [5]. This targeted approach, compared to other structural elements, underscores its simplicity and potency. The repercussions of such detonations on slabs often surpass those of close-in blasts, as the concentrated explosive energy magnifies the likelihood of substantial structural impairment [5,6]. Safeguarding these slender, flexural structural components against explosive forces is imperative for upholding the structural integrity and safeguarding the occupants and assets within buildings [5]. Hence, instituting measures to fortify and attenuate the impact of explosive forces on slabs stands as an essential endeavor in fortifying structures against potential threats.

In recent years, scholars [3–15] have delved into a plethora of external and internal mitigation strategies aimed at augmenting the resilience of slabs against explosive forces. These include the utilization of advanced materials such as CFRP laminates, steel sheets, and CFRP bars, as well as the implementation of sophisticated reinforcement techniques such as two-layer reinforcement and high-strength concrete [6–15]. Additionally, shock-absorbing materials, fiber-reinforced concrete, and innovative anchorage systems have been investigated for their potential to enhance blast resistance [6–15]. However, the current investigation introduces a pioneering methodology centered on the integration of vertical short bars, colloquially known as studs, which are welded with the reinforcement, to bolster the anti-contact-explosion capabilities of slabs. These studs are strategically positioned on various facets of the slab, including the compression face, tension face, or both, deviating from traditional reinforcement methodologies. The novelty of this research lies in its targeted application of studs to address the unique challenges posed by contact blasts, thereby offering a promising avenue for advancing the discipline of structural engineering in the realm of blast protection.

Although conducting experimental trials on slabs subjected to blast loading is crucial for understanding their structural dynamics and assessing their resilience against explosions, this numerical-only study, validated against experimental data in the literature, provides reliable insights into their behavior under such conditions [2,3]. These trials furnish invaluable insights into material behaviors under blast waves, facilitating the advancement of more robust structural frameworks. However, such trials are frequently im-

peded by a plethora of constraints. Factors such as restricted availability of suitable testing locales, exorbitant expenses associated with transporting specimens to these locales, and the necessity to procure heavy machinery for test setups present formidable hurdles [1,2]. Furthermore, the intrinsic hazards inherent in blast testing introduce an additional stratum of intricacy and peril. To surmount these limitations, numerical simulations employing rigorously validated models have emerged as a feasible and economical alternative [1]. By harnessing computational analyses, researchers can replicate blast scenarios, anticipate material reactions, and visualize stress distributions within the slabs. Additionally, numerical simulations afford flexibility and scalability, enabling experimentation under diverse conditions devoid of the logistical encumbrances inherent in physical testing [1,2].

Furthermore, experimental investigations encounter additional hurdles, including adherence to stringent safety protocols and compliance with environmental regulations, thereby heightening the complexity of the endeavor [1–3]. Moreover, the inherent variability in experimental conditions, attributable to uncontrollable variables such as inclement weather or equipment malfunctions, introduces a level of uncertainty into the obtained results. Additionally, the dearth of academic curricula addressing blast engineering exacerbates the situation, resulting in a scarcity of both expertise and resources devoted to conducting such experiments. Moreover, logistical challenges, including limited access to specialized equipment and facilities, as well as the substantial time and resources required for coordination and execution, further impede experimental studies. Conversely, numerical simulations offer a viable alternative with fewer encumbrances. Through meticulous validation against empirical data, these simulations provide a controlled setting wherein parameters can be precisely manipulated, scenarios replicated consistently, and results garnered with heightened efficiency. Consequently, researchers can explore a broader spectrum of scenarios and design iterations within compressed timeframes, culminating in a more exhaustive comprehension of the structural response to blast loading. Given the challenges inherent in accessing testing sites and the paucity of laboratory infrastructure in academic institutions, the authors of this investigation have embraced numerical simulation methodologies to prognosticate the anti-blast performance of slabs, facilitating efficient and comprehensive analyses within controlled environments. The authors have employed a versatile, high-fidelity physics-driven finite element tool, namely, Abaqus [16], to meticulously simulate and analyze the impact of blast loading on slabs.

Experimentally tested, the slab model meticulously examined by Zhao et al. (2019) [3], composed of standard concrete and reinforced solely with one-mesh re-bars measuring 6 mm in diameter spaced at 75 mm center-to-center (c/c), garners recognition as a benchmark reference in this research work. Its validation, achieved through rigorous experimental testing and meticulous analysis utilizing the Eulerian–Lagrangian method coupled with finite element formulation in the Abaqus tool, guarantees its reliability. Building upon this validated model, further investigation is undertaken to explore the impact of studs and their application in augmenting the anti-blast efficacy of the slab. This expansion of the research endeavors to furnish valuable insights into the optimization of structural robustness and the resilience of concrete slabs under blast loading conditions.

In consideration of the formidable fiscal burdens associated with conducting live explosion trials, a considerable cohort of researchers has elected to employ a fusion of delimited experimental endeavors and sophisticated computational methodologies. This strategic choice not only serves to curtail research outlays but also enables the undertaking of comprehensive analyses, delving into the intricate response dynamics of structural constituents when subjected to blast loading scenarios meticulously replicated through numerical simulations. Table 1 provides a succinct overview of studies delving into slab dynamic behavior and blast resistance, showcasing diverse approaches and insights within the field.

Table 1. Compilation of scholarly studies exploring slab dynamic behavior and blast resistance.

Researchers	Study Summary
Huff [17]	The objective of this investigation was to elucidate the response, culminating in structural failure, of a conventional flooring and framing configuration prevalent atop a subterranean refuge beneath a steel-framed construction. Static and dynamic examinations were conducted on two scaled-down models, at a ratio of 1:4.5, representing the subterranean shelter space extrapolated from a prototype multistory steel framework specifically crafted for this research endeavor.
Silva and Lu [18]	This work evaluated the effectiveness of composite materials in augmenting the blast resilience of slabs. Experimental analysis unveiled the fact that slabs reinforced on dual facets exhibited notable enhancement in blast resistance, primarily stemming from adverse moments generated by blast dynamics. Furthermore, a tailored displacement-driven approach accurately predicted blast loads, corroborated by closely aligned damage patterns, with anticipated outcomes.
Lan et al. [19]	This manuscript delineated a comprehensive examination regimen concerning composite structural elements subjected to explosive forces. Seventy-four specimens, encompassing slabs and sandwich panels, underwent scrutiny utilizing charges varying between 8 and 100 kg. Variables under scrutiny comprised material composition, thickness, airblast overpressure, accelerative forces, and peak displacement. Additionally, detailed documentation of failure modalities was conducted for each specimen category.
Zhou et al. [20]	The research employed a dynamic plasticity damage paradigm to scrutinize the blast reactions of slabs, incorporating tailored strength and damage formulations. It executed three-dimensional simulations following antecedent two-dimensional modeling, juxtaposing outcomes against the benchmarks delineated in TM5-1300 specifications.
Tanapornraweekit et al. [21]	A 5000 kg TNT blast in Woomera, South Australia, tested a panel. Advanced computational algorithms prognosticated the blast repercussions, whereas LS-DYNA meticulously simulated the dynamic intricacies of the panel. Validation against empirical data unequivocally showcased the software's precision in mirroring the panel's reactive tendencies.
Lu [22]; Schenker et al. [11]; Wu et al. [14]; Thiagarajan et al. [13]	Examined cutting-edge technologies designed to enhance the deflection capabilities and reinforce the damage resilience of slabs exposed to explosive forces.
Hao et al. [23]	The paper analyzed how RC slabs respond to blast loading and factors influencing them. It created a numerical model considering strain rate effects and damage accumulation, and then proposed blast-resistant design principles.
Ohkubo et al. [24]	The study tested carbon and aramid fiber-sheet reinforcement on concrete plates against explosions, finding significant reduction in damage and prevention of fragmentation.
Zhou and Hao [25]	A mesoscale concrete model intricately replicated the dynamic collapse resulting from contact detonation within a slab, taking into account the presence of high-strength coarse aggregates juxtaposed with a low-strength mortar matrix. Employing an integrated dynamic plastic-damage material model within AUTODYN, it meticulously juxtaposed two stochastic aggregate arrangements against outcomes derived from a uniform model, thereby conjecturing the distributions of fragment sizes.
Morales et al. [26]	Blast loading experiments have enhanced the sophistication of numerical methodologies for simulating the behavior of concrete subjected to explosive forces. The concurrent examination of four distinct concrete specimens was facilitated, with a total of twelve slabs subjected to four controlled-detonation trials. The findings were corroborated through rigorous simulations, with the experimental setup meticulously designed to mitigate dispersion and economize resources. It was discerned that the tensile strength predominantly dictates the capacity of structures to withstand blast pressures.
Zhao and Chen [27]	This investigation scrutinized the dynamic response of three slabs to proximal detonations. Employing LS-DYNA software, computational simulations were juxtaposed with empirical tests. Findings evinced concordance between computational models and empirical observations, underscoring the robustness of the predictive capacity of the model in delineating structural damage and discerning the influence of explosive magnitude on failure mechanisms.

Table 1. Cont.

Researchers	Study Summary
Wang et al. [28]	The investigation delved into the impact of blast loads on reduced-scale slabs. The results elucidated two tiers of impairment: negligible spalling and intermediate spalling. While the macroscopic structural deterioration remained uniform, the slabs with greater magnification ratios exhibited marginally diminished localized harm. Two formulae were proposed to calibrate outcomes when transitioning from the model to the full-scale prototype.
Zhao et al. [29]	This study delved into the reaction of containment structures to internal blast phenomena utilizing LS-DYNA simulation software. Its primary focus lay in elucidating the intricate damage mechanisms at play, while meticulously scrutinizing the impact of varying scale distances and mesh attributes on the structural resilience against explosive forces.
Wu et al. [14]	Two RC specimens underwent explosive testing: one unmodified, the other retrofitted with six NSM CFRP plates. Both endured 2.1 kg TNT detonation from 0.6 m, causing concrete scabbing. Fragment analysis showed size distributions adhering to Weibull and RRSB patterns, while shape factors followed a lognormal distribution. The study evaluated the fragment size's impact on energy density dissipation.
Wang et al. [28,30] and Zhang et al. [31]	The investigations meticulously examined the modes of degradation demonstrated by slabs and beams exposed to diverse detonations. Additionally, it introduced a novel damage assessment framework, employing the SDOF method.
Lin et al. [10]	An LS-DYNA model simulated blast responses of steel-reinforced concrete panels, analyzing element size effects, validating with experimental data, and studying blast resistance factors parametrically.
Castedo et al. [32]	The study validated a blast simulation model against field tests for full-scale slabs. Results highlighted sensitivity to scaled distance and construction methods, with slabs incorporating fibers showing superior blast resistance.
Qu et al. [33]	Numerical studies explored blast effects on pre-cracked RC beams, revealing increased deflection and stresses, with premature failure at crack sites. Compression zone cracks had significant impact; damage was localized, and crack dimensions minimally affected beam behavior.
Li and Hao [6]	This study delved into the behavioral dynamics of slabs under the duress of TNT detonations. Employing sophisticated computational algorithms, the study embarked on a series of simulations to scrutinize diverse detonation scenarios, elucidating their resonance with resultant structural impairments. The findings adeptly anticipated apex pressure thresholds and authenticated the emergence of fracture configurations, thereby enhancing our comprehension of blast-induced phenomena.
Yao et al. [34]	The investigation scrutinized concrete slabs featuring varying reinforcement ratios subjected to explosive forces. It elucidated that augmenting the explosive charge exacerbated structural harm, whereas elevated reinforcement ratios mitigated both damage and deflection. Such findings underscore the paramount importance of the reinforcement ratio in bolstering the resilience of slabs amidst blast scenarios.
Zhao et al. [35]	An assessment was conducted on the blast resilience of 60-degree reinforced concrete slabs by a proficient model, juxtaposing them with their conventional counterparts. The analysis delved into variables such as slab thickness and the magnitude of the explosive charge, while also advancing prognostic methodologies tailored to anticipate blast resilience.

The chief objectives delineated in this paper are as follows:

- Authenticate the slab model via mesh refinement analysis and juxtaposition with extant findings reported in [3].
- Explore the efficacy of incorporating studs, affixed through welding with the upper and lower bars, as well as both, to augment the slab's resistance to a touch-off explosion.
- Scrutinize the influence of stud elevation on the structural response of the slab to blast-induced damage.

In a previous investigation conducted by Zhao et al. (2019) [3], the researchers employed a thin plate with studs, representing conventional reinforcement, embedded within the slab under contact explosions. However, this approach yielded subpar results com-

pared to conventional slabs in terms of structural damage [3]. In the present study, the authors have innovatively employed welded studs in conjunction with the reinforcement bars, which allows the continuity of mechanical interlocking of the coarse aggregate of the concrete; this is further confined by the projecting studs welded with the re-bar layer, thereby addressing the discontinuity of the concrete by the steel plate which is made to develop a weak adhesive force between the bottom face of the plate and the concrete—a serious shortcoming of the previous research endeavor [3]. Under contact explosion, this adhesion fails during the reflected tensile stress wave, resulting in its detachment from the plate, as observed in [3].

2. Understanding Blast Loading Mechanisms and Design Limitations

Blast loading, marked by a sudden discharge of energy, imposes substantial pressure on adjacent structures, presenting considerable challenges to their structural integrity [2]. Figure 1 portrays a customary blast pressure profile, illustrating the chronological sequence of events as the blast wave traverses a specified locus. Subsequent to the impact, atmospheric pressure undergoes an abrupt escalation either to the zenith of incident pressure (P_{so}) or the pinnacle of reflected pressure (P_r), contingent upon the existence of reflective surfaces. “ t_a ” represents the time of arrival. The positive phase of the blast, denoted by t_d^+ , signifies the period during which pressure exceeds atmospheric norms, while the negative phase, spanning t_d^- , delineates the duration during which overpressure subsides beneath atmospheric thresholds.

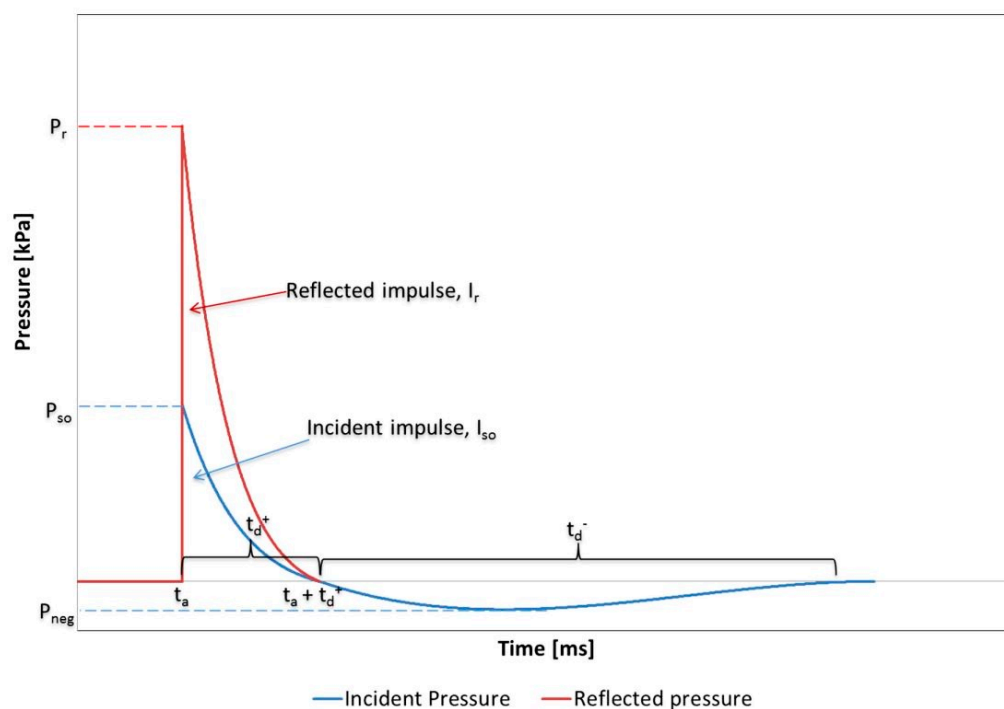


Figure 1. Standardized TNT blast profile and lexicon.

In spite of the critical significance of blast loading, prevailing design standards and manuals [1,2] are deficient in providing adequate measures to confront the distinctive challenges posed by such dynamic occurrences. This insufficiency can be attributed chiefly to the intricate and variable nature of blast loading scenarios, influenced by a multitude of factors including proximity to the explosion, size of the explosive charge, surrounding topography, and structural configuration [1–5]. Moreover, the dynamic character of blast loading renders the formulation of universally applicable design protocols arduous, given the diverse spectrum of encountered scenarios [1,2]. Consequently, engineers frequently resort to empirical methodologies or excessively cautious strategies, potentially

resulting in either excessive fortification or underestimation of structural blast resistance. Consequently, there exists a pressing necessity for intensified research and development endeavors directed towards refining blast loading models and delineating comprehensive design principles, ensuring the safety and robustness of infrastructure and facilities in the event of blast occurrences.

Advanced numerical blast techniques, such as the Eulerian–Lagrangian approach [2,3,5], coupled with the finite element method, present promising solutions for rectifying deficiencies in conventional design standards. This sophisticated approach facilitates the precise simulation of explosion events and the prediction of structural responses and damages. The Eulerian–Lagrangian approach achieves this by dividing the computational domain into distinct Eulerian and Lagrangian zones [16], allowing for the comprehensive modeling of blast waves and their interaction with structures. Within this framework, the Eulerian component captures the propagation of blast waves through the surrounding medium, while the Lagrangian component monitors the motion and deformation of individual structural elements [2,3]. Moreover, by integrating intricate material models and blast loading profiles obtained from experimental data, the finite element method ensures accurate representation of the dynamic behavior exhibited by structures subjected to blast loading conditions.

3. General Response of Slabs to Touch-Off Explosions

The response of a slab to a touch-off explosion manifests as an intricate amalgamation of multiple phenomena, each exerting influence on the structural integrity and extent of damage sustained.

- Following detonation, the release of explosive energy generates compression waves of high pressure that propagate through the material, inducing significant internal stresses.
- These stresses precipitate various forms of damage within the slab, including rupturing of the reinforcement.
- Reflected waves, generated at the slab's free surface or back end, interact with incident waves, exacerbating the destructive impact.
- A common outcome is perforation, where blast pressure surpasses material strength, leading to localized penetration or through-thickness rupture.
- Cracking arises from fractures within the slab induced by tensile stresses from the explosive shock wave.
- Crushing occurs when compressive forces exceed material capacity, resulting in plastic deformation or catastrophic failure.
- Spalling at the blast front involves the detachment of surface layers due to tensile stresses, often resulting in projectile hazards.
- Conversely, scabbing at the remote face of the slab occurs when fragments are forcefully ejected, posing risks to surrounding areas.

Modes of Failure for Slabs

Table 2 delineates diverse modalities of failure that slabs may experience when exposed to initiation detonations, accompanied by concomitant patterns of impairment. Proficiency in discerning these modalities can enrich architectural schematics and defensive protocols aimed at ameliorating the ramifications of explosive forces on edifices and civil works. This table has been compiled based on a thorough review of past publications referenced by the cited researchers [1–11].

Table 2. Modes of failure for slabs with corresponding conditions of damage.

Mode of Failure	Description	Conditions of Damage
Flexural Mode	The structural integrity of the slab is compromised as it succumbs to bending stresses induced by the force of the explosion, manifesting in the formation of cracks and fractures spanning the entirety of its length or width.	<ul style="list-style-type: none"> • A significant magnitude of explosive force is directed precisely beneath the central region of the slab. • There exists a considerable dissonance between the compressive and tensile strengths inherent in the material constituting the slab.
Flexure-Shear Mode	The amalgamation of flexural and shear failure manifests as the slab undergoing both bending and shear stress concurrently, resulting in a confluence of bending deflection and diagonal cracks.	<ul style="list-style-type: none"> • Explosion characterized by a substantial lateral force component. • Slab configuration susceptible to heightened stress concentration at corners or edges.
Shear Mode	Shear failure transpires when the slab undergoes forces that prompt the internal strata of the material to glide in a way relative to each other, culminating in the emergence of diagonal cracks or complete disintegration.	<ul style="list-style-type: none"> • Elevated lateral forces induced by the explosion result in the slab's failure along diagonal planes. • The debilitation or compromise of slab edges stems from antecedent damage or substandard construction quality.
Blast-Induced Spalling	The uppermost stratum of the slab undergoes expulsion owing to intense compressive pressures instigated by the detonation, frequently culminating in formations resembling craters or fragmentations.	<ul style="list-style-type: none"> • The slab surface experiences a rapid and intense application of blast waves, imposing significant pressure. • The manifestation of surface imperfections, including cracks or joints, intensifies the concentration of stress.
Punching Shear	The phenomenon of structural failure occurs when a concentrated force induces shearing stresses along the perimeter of a column or supporting element, leading to the rupture of a slab. This typically manifests as a circular- or diamond-shaped breach in the slab material.	<ul style="list-style-type: none"> • An explosion in close proximity to supporting columns or load-bearing elements exerts concentrated loads upon the slab. • Inadequate reinforcement encircling column–slab connections permits the localized propagation of shear failure.

4. Numerical Modeling of Slab Response to Touch-Off Explosive Events

4.1. Simulation Methodology

The ABAQUS 2020 [16] software suite emerges as a formidable tool for intricately simulating the effects of explosions on slabs. This research initiative commences with modeling the slab, drawing insights from the experimental investigation conducted by Zhao et al. [3]. Utilizing the CEL-FEM technique [3,5,16], the simulation recreates a touch-off explosion scenario, where air and TNT constitute the Eulerian domain, while the slab embodies the Lagrangian structure of interest, shown in Figures 2 and 3. The interplay between the Eulerian and Lagrangian meshes assumes paramount importance: the Eulerian mesh imposes a pressure boundary upon the Lagrangian counterpart, inducing displacement akin to slabs, whereas the Lagrangian mesh reciprocally enforces a velocity boundary upon the Eulerian fabric, thereby tethering it in spatial stasis to forestall any infiltration of material. In a bid to augment verisimilitude, an atmospheric zone is seamlessly integrated within the model. The areas countenanced by the Eulerian domain remain immobile, to forestall any exodus of material, with non-reflective Eulerian boundaries meticulously stationed along the lateral confines to obviate the reflections of pressure waves. Furthermore, a rigid substrate is incorporated beneath the domain to emulate the reverberations of blast shockwaves, as illustrated in Figure 2. The pneumatic pressure within the atmospheric domain is calibrated to mirror that of the atmosphere, while the two opposing sides of the RC slab are endowed with clamped supports. Through this comprehensive simulation framework, Abaqus facilitates a meticulous exploration of blast effects on slabs with unparalleled fidelity.

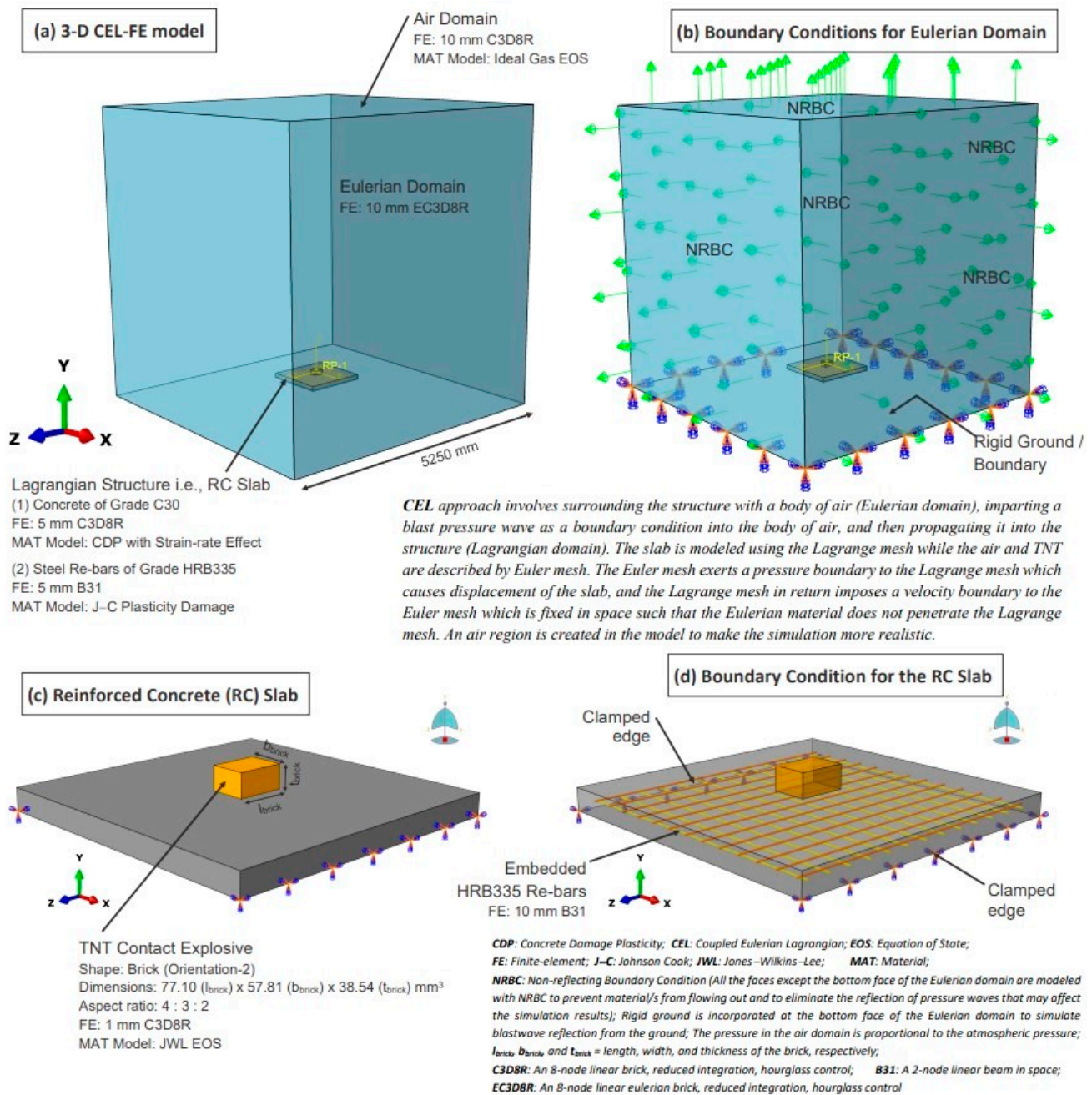


Figure 2. Computational framework.

This research endeavors to bolster urban infrastructure against the destructive impact of bombings by introducing vertical studs into concrete slabs, presenting a novel, resource-efficient methodology. The incorporation of these vertical studs is aimed at augmenting the structural robustness of the concrete slabs by efficiently dispersing and dissipating the energy released during explosive incidents. Through the strategic positioning of these studs within the concrete framework, we envisage a substantial reduction in damage inflicted by blasts, as these studs serve as pivotal reinforcement points, redirecting forces and curtailing the spread of cracks. This pioneering approach not only fortifies the concrete slabs but also minimizes the requisite additional material, rendering it a cost-effective solution for enhancing the resilience of urban infrastructure to explosive threats.

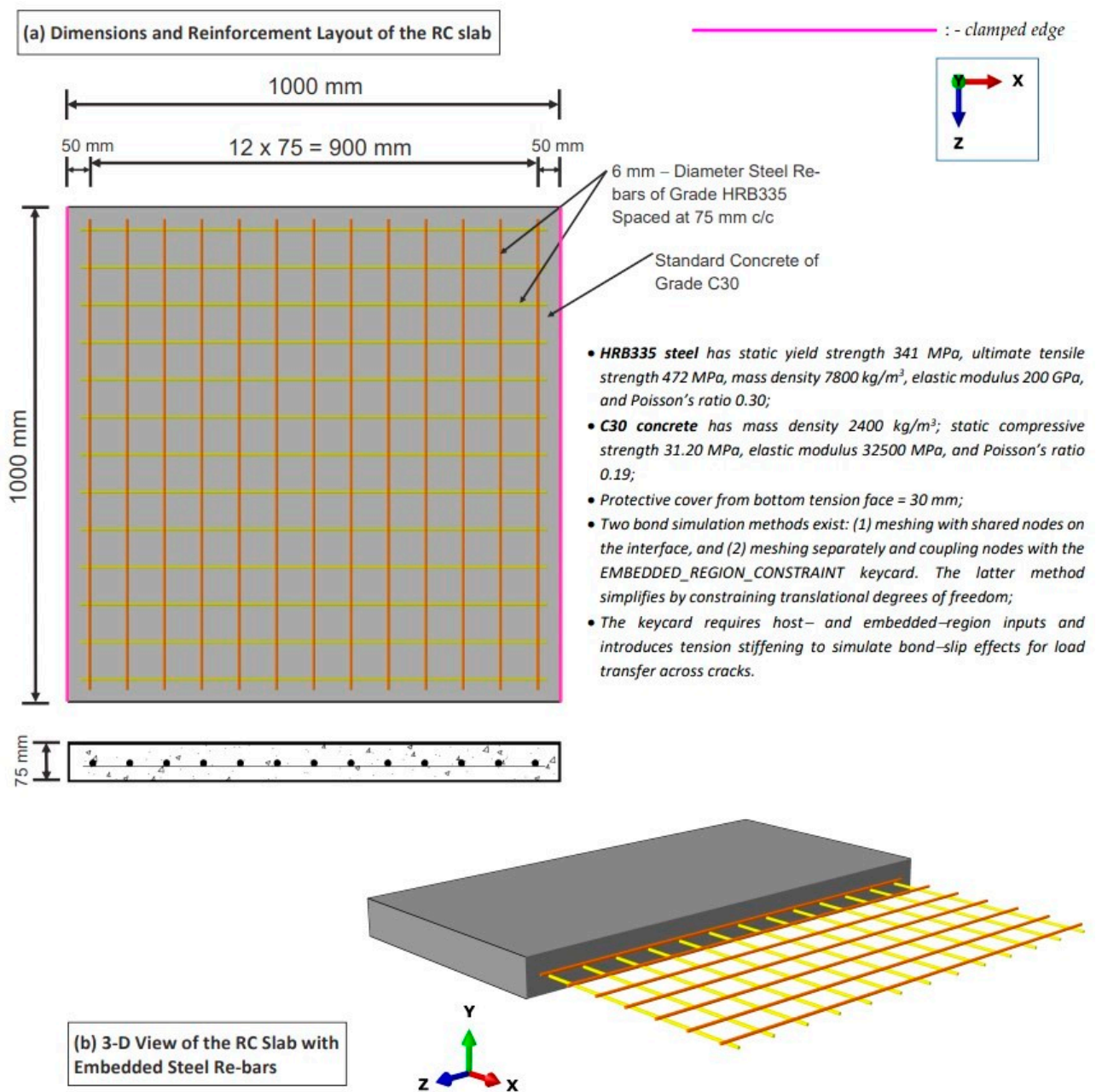


Figure 3. Properties of the slab materials.

Altogether, seven distinct slab models have been generated utilizing the software platform. Among these, one slab functions as the control variant, devoid of studs, whereas the remaining six variants incorporate studs of diameter 6 mm and of varying heights: 15 mm and 10 mm, see Figure 4. Additionally, each of these six configurations is further distinguished by the welding arrangement, encompassing options including (i) solely upper-layer bars, (ii) exclusively bottom-layer bars, and (iii) both upper- and bottom-layer bars. The studs possess identical material properties to the steel bars employed. Notably, the control variant features a bottom clear cover of 30 mm, whereas in slabs incorporating re-bars and studs, this dimension is reduced, assuming the minimum aggregate thickness of concrete to be 10 mm.

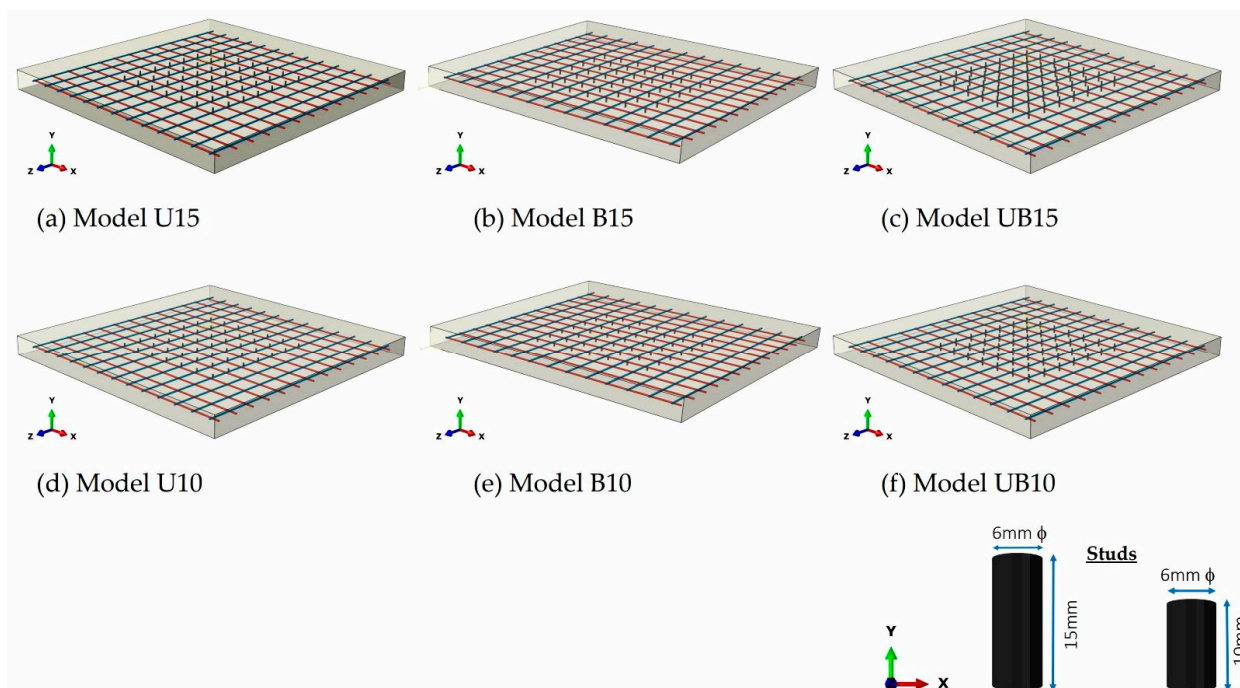


Figure 4. Slabs with studs.

Below are the designations assigned to the models developed as part of this research endeavor (Figure 4).

- **Model N:** Slab without studs. This model represents the baseline configuration without any studs welded to the reinforcement bars.
- **Model U15:** Studs welded with upper layer bars, height = 15 mm.
- **Model B15:** Studs welded with bottom layer bars, height = 15 mm.
- **Model UB15:** Studs welded with both upper- and bottom-layer bars, height = 15 mm.
- **Model U10:** Studs welded with upper-layer bars, height = 10 mm.
- **Model B10:** Studs welded with bottom-layer bars, height = 10 mm.
- **Model UB10:** Studs welded with both upper- and bottom-layer bars, height = 10 mm.

It is imperative to acknowledge that the anchoring elements (studs) within the slabs have been strategically positioned solely within a central portion spanning $450\text{ mm} \times 450\text{ mm}$, maintaining a clearance of 275 mm from all sides of the square slab. This decision is predicated upon two primary considerations: firstly, the anticipated blast scenario involves a touch-off explosion, thereby confining the resultant response to a more localized area within the explosive region; secondly, the authors seek to avoid a substantial augmentation of the steel reinforcement ratio within the slabs. The initiation of a detonation, either through touch-off or contact, at the central point of the slab, induces a localized response characterized by the occurrence of punching, perforation, concrete scabbing, and deformation of the reinforcing bars within the delineated blast zone. Thus, the authors have employed studs within this specifically affected blast or impacted area. However, it is paramount to underscore that in the event of an eccentric or off-center blast detonation, the positioning of studs throughout the entirety of the slab would be deemed more prudent. Such a strategy ensures the comprehensive fortification of the structure against potential blast-induced effects spanning the entire expanse of the slab.

In computational simulations employing software such as Abaqus [16], the tie constraint directive is frequently utilized to emulate the fusion of studs onto reinforcement bars within reinforced concrete structures. This constraint establishes a kinematic correlation between two surfaces or nodal points, effectively amalgamating them to emulate welded junctions within the tangible framework. When implemented to replicate stud welding, the tie constraint conjoins the nodal points representing the stud and the re-bar, ensuring their synchronous movement as a singular entity when subjected to loading. This

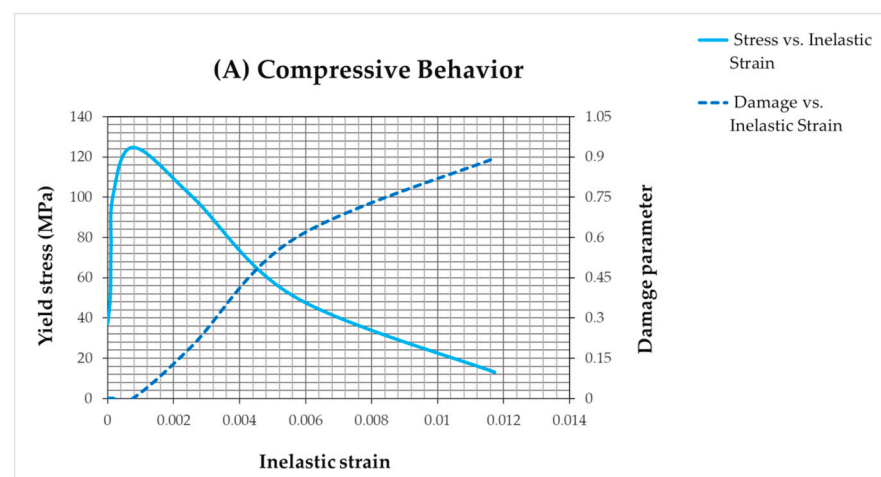
constraint adeptly transmits forces between the stud and the reinforcement, facilitating simulations that accurately depict the structural reactions to diverse loading scenarios, including touch-off explosions, with exceptional precision.

4.2. Modeling Concrete Damage with Abaqus CDP and Incorporating Strain Rate Effects

The Concrete Damage Plasticity (CDP) [16] model embedded within the Abaqus software has demonstrated remarkable efficacy in prognosticating concrete deterioration amid touch-off explosion scenarios, as corroborated by antecedent research endeavors. This model adeptly accommodates the intricate nonlinearities inherent to concrete materials, encompassing the evolution of damage and structural failure by amalgamating plasticity theory with damage mechanics. Fundamentally, the CDP model conceptualizes concrete as a substance capable of manifesting both elastic and plastic deformation, with damage propagation being contingent upon stress levels. To address the influence of strain rate fluctuations in dynamic scenarios, dynamic increase coefficients (DICs) are integrated into the CDP framework. In this specific work, the amplification of DICs induced by the influence of strain rate was meticulously regulated and upheld at a consistent level. The calibration procedure involved an initial application of static reference mechanical attributes, which were subsequently fine-tuned to align seamlessly with experimental observations. Despite the inherent simplifications, the outcomes derived from this methodology closely align with findings from antecedent research on concrete specimens [1,5,36], where DIC values pertaining to compressive strength (f_c), tensile strength (f_t), and Young's modulus (E_c) typically reside within the range of 3 to 6. Table 3 encapsulates the resultant dynamic properties alongside their corresponding DIC values, while acknowledging the constant nature of the DIC throughout the analysis. Figure 5 illustrates the relationship curves displaying the calibrated final values of the CDP constituent model.

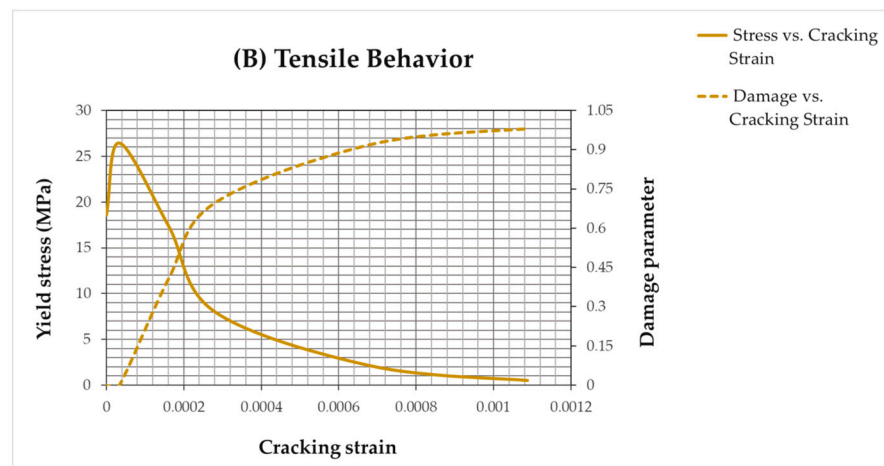
Table 3. Dynamic concrete properties.

Strength Parameters	Initial	Final	DIC
f_t (MPa)	3.10	1.86×10^1	6
f_c (MPa)	3.12×10^1	1.248×10^2	4
E_c (GPa)	3.25×10^1	9.75×10^1	3



(a) Relationships among the compressive stress, inelastic compressive strain, and compressive damage factor

Figure 5. Cont.



(b) Relationships among the tensile stress, cracking strain and tensile damage factor

Figure 5. Graphs illustrating the correlation curves (final calibrated values) of the CDP constituent model.

In light of the extensive utilization of the CDP model by a multitude of researchers within blast scenarios and its proven alignment with previous experimental outcomes, it has been integrated into this study.

4.3. Role of Element Type and Mesh Size in Finite Element Analysis (FEA)

In FEA, the decision regarding element type and mesh size holds significant sway over the precision of outcomes and computational efficacy. Optimal selection of elements is pivotal in faithfully portraying the behavior of materials under scrutiny. Furthermore, mesh size directly dictates the granularity of details captured in the analysis, with finer meshes typically affording greater precision albeit at the expense of heightened computational demands. Additionally, ensuring the compatibility of chosen elements with the designated material model is imperative for attaining desired simulation accuracy. In the current investigation, meticulous attention is directed towards the choice of elements for modeling both concrete and reinforcement bars. The C3D8R element is enlisted to represent the concrete, while the B31 element is adopted for modeling the reinforcement bars. Extensively employed by prior researchers, these elements are acclaimed for their computational efficiency and accuracy. Moreover, the atmospheric domain and the TNT dose are discretized using C3D8R, thus ensuring methodological consistency throughout the analysis.

4.4. Johnson Cook Plasticity Damage (JCPD) Model for Steel

The JCPD [16] model finds widespread application within Abaqus software for simulating the response of steel across diverse loading scenarios. This model integrates intricate mechanisms aimed at capturing the material's behavior, particularly when subjected to high strain rates and elevated temperatures. Parameters such as strain rate sensitivity, thermal softening, and damage evolution are meticulously accounted for, enabling precise simulation of the material's response. As reported by Zhao et al. [3], the static yield strength of the steel grade under consideration stands at 341 MPa, accompanied by an ultimate tensile strength of 472 MPa. Moreover, the material exhibits a mass density of 7800 kg/m³, an elastic modulus of 200 GPa, and a Poisson's ratio of 0.30. Lin et al.'s experimental investigation [37] furnishes additional material parameter values pertinent to steel of grade HRB335. To enhance the model's accuracy in blast response simulations, a bending DIC of 1.25, as per UFC 3-340-02 (2008), is employed.

4.5. Modeling the Concrete–Steel Bond

Within Abaqus, the interface between concrete and bars of steel is commonly modeled by discretizing the concrete and embedded components independently and subsequently coupling the corresponding nodes utilizing the default embedded constraint [16]. This method entails delineating the host region (comprising the concrete component) and the embedded region (housing the bars) within the embedded region of the meshed parts [16], see Figure 3. To emulate the phenomenon of bond-slip occurring at the interface between steel and concrete, a technique known as tension stiffening is employed [1,16]. Tension stiffening serves to capture the transfer of loads through reinforcement bars across cracks in the concrete, effectively simulating the intricate interaction between these two materials [16].

4.6. Equation of States (EoS)

In the simulation of explosive events within the Eulerian domain using Abaqus, the choice of EoS assumes paramount significance in accurately encapsulating the dynamics of the involved materials. While air, often idealized as an inert gas, is typically modeled using the Ideal Gas EoS, which posits that air molecules behave as isolated entities devoid of intermolecular interactions and volume considerations, explosive substances such as TNT exhibit intricate thermodynamic characteristics necessitating a more nuanced EoS. The Jones–Wilkins–Lee (JWL) EoS, frequently employed for explosives [3,5,6,16], accommodates phenomena like shock wave propagation and chemical transformations. Within the current simulation paradigm, Abaqus draws upon its material library [16] to access standard air constants, ensuring uniformity and dependability. Moreover, the specific energy of air, assumed at 2.068×10^5 kJ/kg, serves as a fundamental parameter for the blast event simulation. These judicious selections collectively facilitate the precise representation of both air and TNT within the computational framework, a prerequisite for accurate prognostication of blast dynamics and their consequential structural ramifications.

$$P = A \left(1 - \frac{\omega\rho}{R_1\rho_0} \right) e^{-\frac{R_1\rho_0}{\rho}} + B \left(1 - \frac{\omega\rho}{R_2\rho_0} \right) e^{-\frac{R_2\rho_0}{\rho}} + \omega\rho E \quad (1)$$

In the current investigation, the pressure emanating from the detonation of the contact explosive, TNT, is meticulously characterized utilizing the JWL-EoS. This formula, designated as Equation (1), serves to model the hydrostatic pressure (P) engendered by the explosive substance. It integrates a range of user-defined material constants, namely, A , B , R_1 , R_2 , and ω , each playing a distinct role in shaping the pressure generation mechanism. These constants are meticulously calibrated through empirical observations and prior experimental studies [2,3,5]. In this specific simulation scenario, the constants assume the following values [3]: $A = 373.77$ GPa, $B = 3.7471$ GPa, $R_1 = 4.15$, $R_2 = 0.90$, and $\omega = 0.35$. Furthermore, ρ_0 signifies the user-defined density of the explosive material (kg/m^3), whereas ρ denotes the density of the explosive material itself, fixed at $1630 \text{ kg}/\text{m}^3$ within this context. Additionally, E symbolizes the explosion energy per unit mass, set at $4905 \text{ kJ}/\text{kg}$. By meticulously incorporating these parameters into the JWL-EoS, the simulation adeptly captures the intricate pressure dynamics ensuing from TNT detonation, thereby facilitating precise predictions of blast effects and their repercussions on adjacent structures.

It is imperative to acknowledge that the authors have provided only broad outlines of the materials' properties in this current study. Elaborate descriptions of the materials, encompassing their characterization and parameters, can be found in their previously disseminated research [5]. This strategy is implemented to mitigate potential concerns regarding redundancy and to forestall unnecessary duplication of data. By leveraging their earlier investigations [5], the authors uphold transparency and preserve the integrity of their scholarly endeavor, directing their attention towards the precise facets of the current simulation.

The subsequent sections of the manuscript delve into mesh refinement analysis, verifying the computational framework, scrutinizing results, and elucidating significant findings and recommendations.

4.7. Mesh Refinement Analysis and Model Validation

The process of mesh refinement analysis holds paramount importance in the validation of numerical outcomes vis-à-vis experimental data, as it underpins the precision and dependability of computational simulations. Within this methodology, diverse element sizes are scrutinized, juxtaposed against experimental findings to discern their congruence. In the present work, the empirical observations by Zhao et al. [3] pertaining to slab deformation and structural impairments serve as a reference point for evaluating computational outputs. Through the segmentation of slab materials into varying element dimensions—wherein 5 mm denotes the finest, while 10 mm and 15 mm represent intermediate gradations, and 20 mm signifies a coarser delineation—a holistic comprehension of the numerical model’s faithfulness is attained. This methodological approach enables researchers to ascertain the optimal mesh size requisite for precise emulation of physical phenomena, thus augmenting the credibility of computational outputs and expediting judicious decision making in structural analysis and design endeavors.

Alterations in the element size prompt divergent responses within the slab, as illustrated in Figure 6. For instance, employing a 5 mm dimension yields a maximum deformation of 48.55 mm, representing a mere 0.92% deviation from experimental observations. Conversely, the utilization of a 20 mm size results in a more pronounced deformation of 53.57 mm, indicating a significant 9.32% increase compared to experimental findings. Intermediate gradations elicit moderate distortions, culminating in peak distortions registering at 50.76 mm (roughly 3.59% in excess of test values) and 51.34 mm (approximately 4.77% higher than test values), respectively. Consequently, a 5 mm size proves optimal, closely simulating the slab’s behavior under blast conditions with minimal variance. Notably, location A2 in Figure 6 corresponds to the centroidal position of the slab’s upper surface, aligning with the region examined in the referenced Study [3]. Additionally, damages observed on the slab, including crack sizes and perforations detailed in Figure 7, closely mirror findings in Reference [3]. Stressing precision, the present study underscores the necessity of employing a 5 mm size for accurate results. It is imperative to emphasize that the slight disparities observed between experimental and computational findings stem from multifaceted factors, encompassing idealizations inherent in material modeling, boundary conditions, and the omission of weather-related effects from consideration.

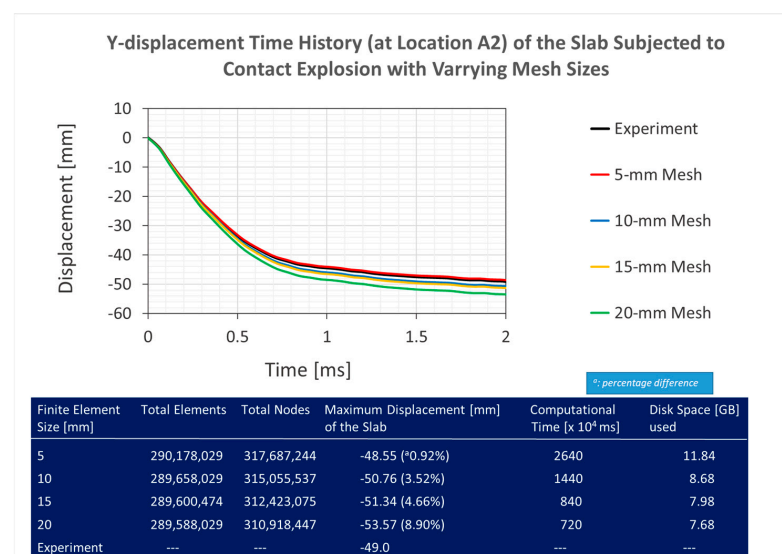


Figure 6. Refinement of mesh analysis: Part I.

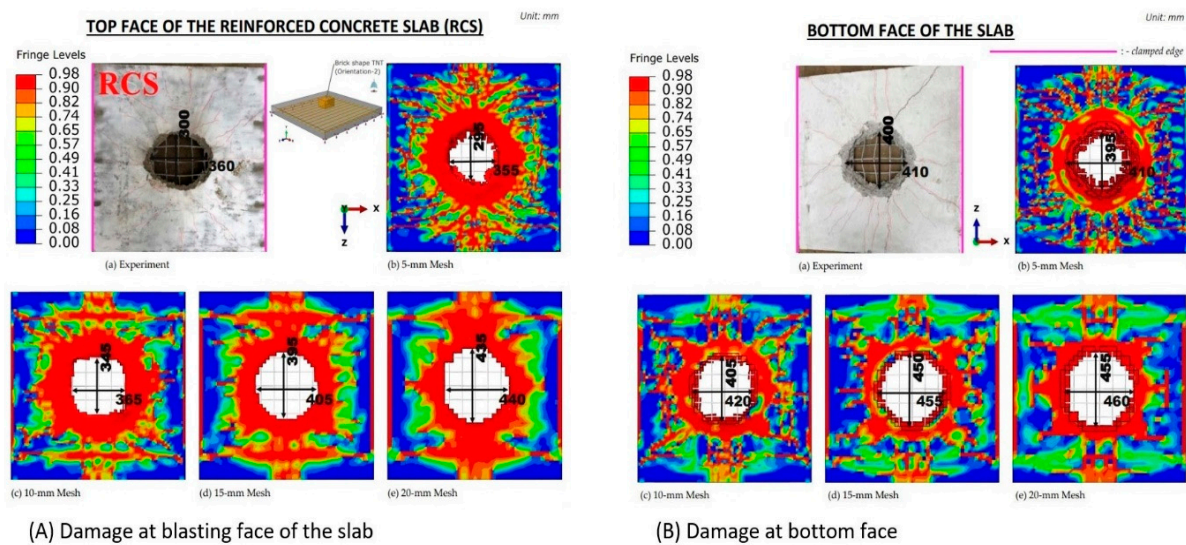


Figure 7. Refinement of mesh analysis: Part II.

5. Results

Studs welded with the upper-layer bars only (Model U15):

- Partial Support:** In this configuration, studs are welded solely to the upper layer bars, providing support primarily to the top surface of the slab. While it offers some enhancement over the baseline, it lacks direct support for the bottom surface, potentially leading to localized plastic strain accumulation upon impact. Consequently, resistance to deformation is not as effective as in configurations with studs on both layers. The deformation in Model U15 is 42.99 mm, representing a reduction of approximately 11.37% compared to Model N (48.55 mm), Figure 8.
- Limited Load Distribution:** As the studs are primarily situated on the top surface, their ability to distribute the explosive load across the slab is restricted. This results in uneven stress distribution, increasing the risk of localized deformation and perforation of the concrete, albeit to a lesser extent compared to the baseline.

Studs welded with the bottom-layer bars only (Model B15):

- Enhanced Load Distribution and Support:** The presence of studs welded to the bottom-layer bars enhances the slab's ability to redistribute the explosive load more uniformly across its thickness. These studs act as anchor points during the explosion, transferring the load to the reinforcement bars and reducing localized stress concentrations. Consequently, this minimizes plastic strain of the concrete. The deformation in Model B15 is 32.96 mm, indicating a reduction of approximately 32.13% compared to Model N (48.55 mm), as well as compared to Model U15 (42.99 mm), Figure 8.
- Improved Resistance to Deformation:** With studs on the bottom layer, the slab gains additional support, enhancing its resistance to deformation. As explosive forces attempt to deform the slab, the studs resist this deformation by transferring the load to the reinforcement bars. This results in smaller deformations compared to the baseline configuration without studs.
- Reinforcement of Concrete:** Welding studs to the bottom-layer bars reinforces the bond between the concrete and the reinforcement, thereby preventing spalling or perforation of the concrete upon impact. By effectively anchoring the concrete to the reinforcement, this configuration reduces the likelihood of separation or fragmentation, thus enhancing the overall structural integrity of the slab.

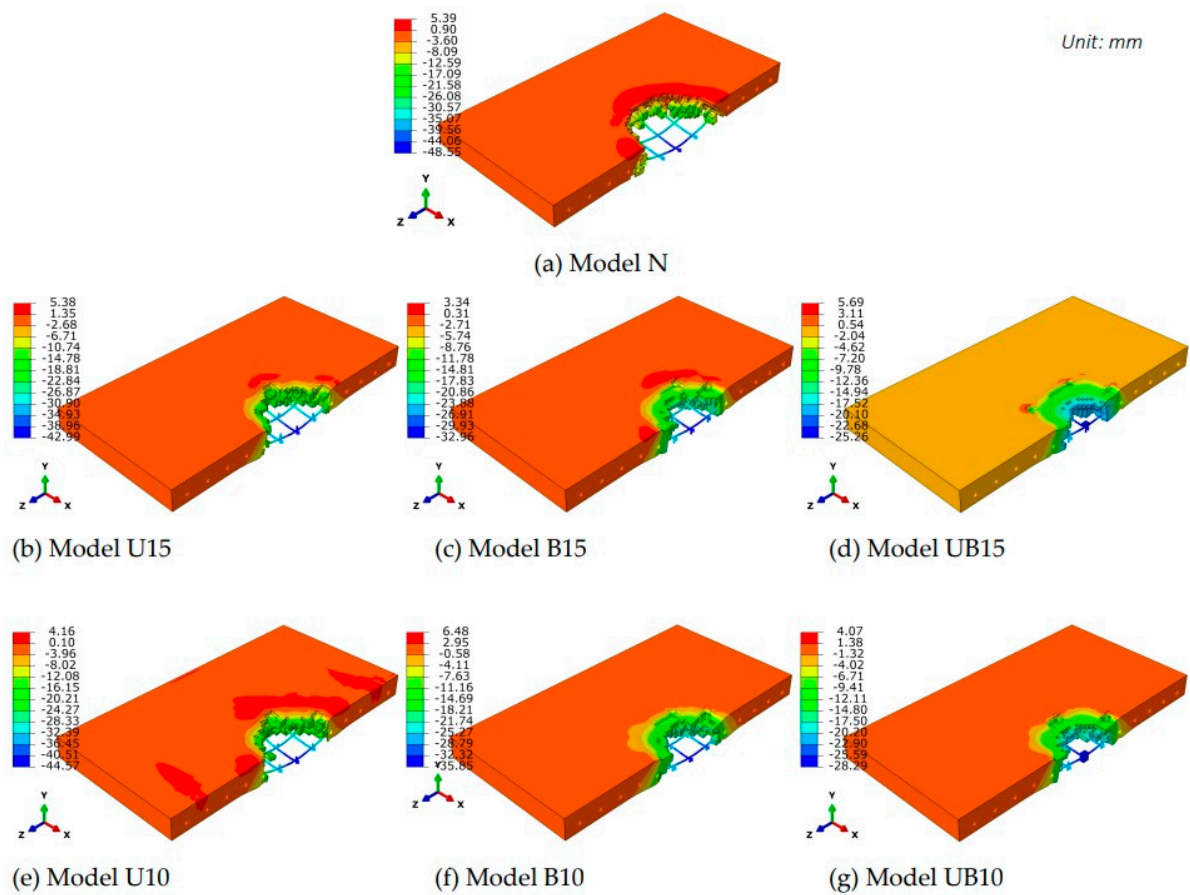


Figure 8. Deformation of the slab materials at $t = 2$ ms.

Studs welded with both upper- and bottom-layer bars (Model UB15):

- *Comprehensive Reinforcement:* Incorporating studs on both layers provides a more comprehensive reinforcement system. Studs on the upper layer offer direct support to the top surface, distributing the load and reducing deformation, while those on the bottom layer reinforce the bottom surface, enhancing resistance to deformation, perforation, and plastic strain. The deformation in Model UB15 is 25.26 mm, showcasing a reduction of approximately 47.91% compared to Model N (48.55 mm).
- *Improved Load Distribution:* With studs on both surfaces, the explosive load is distributed more evenly across the entire thickness of the slab. This results in a more balanced stress distribution, reducing the likelihood of localized deformation and perforation. Additionally, the combined effect of upper- and bottom-layer studs enhances the slab's overall stiffness and strength, further reducing deformation and perforation size.

When comparing the effects of studs with different heights (10 mm versus 15 mm) on the anti-blast capabilities of slabs under touch-off explosions, several key observations emerge.

Studs with a height of 10 mm still contribute to load distribution and support, albeit to a lesser extent than their taller counterparts. However, their reduced height limits their effectiveness in resisting deformation and distributing the explosive load. With less material to anchor the slab to the reinforcement, the shorter studs may experience greater stress concentrations, leading to localized deformation and perforation. Moreover, the shorter studs exhibit diminished resistance to deformation compared to the taller studs. The decreased height reduces their ability to withstand the forces generated by the explosion, potentially allowing for greater deflection of the slab and larger perforation sizes. Additionally, the shorter studs may not provide as strong an anchor for the concrete, increasing the risk of

spalling or separation from the reinforcement, particularly under high-stress conditions. In contrast, studs with a height of 15 mm offer greater load distribution, support, and resistance to deformation. With more material to anchor the slab to the reinforcement, the taller studs distribute the explosive load more effectively, reducing localized stress concentrations and deformation. Their increased height enhances their ability to resist deformation, resulting in smaller deformations and perforation sizes compared to configurations with shorter studs. Furthermore, the taller studs provide a stronger anchor for the concrete, improving the bond between the concrete and the reinforcement. This enhanced connection reduces the likelihood of spalling or separation, contributing to the overall durability and anti-contact-blast capabilities of the slab.

Table 4 presents a summary of the significant dynamic responses computed for the models.

Table 4. Computational results of the slabs.

Model No.	Slab Deformation (mm)	Percentage Reduction (%) with Respect to Control model "N"	Max ^m Tensile Stress (MPa) in the Re-Bars at the Blast Zone	Perforation Dimensions (mm) at the Blasting Face		Perforation Dimensions (mm) at the Remote Face	
				* x	** z	* x	** z
N	48.55	-	812.31	355	295	410	395
U15	42.99	11.45	763.29	320	280	370	295
B15	32.96	32.11	649.67	185	225	330	235
UB15	25.26	47.97	631.80	160	165	200	205
U10	44.57	8.19	756.44	335	285	385	310
B10	35.85	26.15	722.82	205	230	345	245
UB10	28.29	41.73	734.15	175	195	225	215

Note: * dimension corresponds to the free edge; ** dimension corresponds to the restrained edge.

In Figure 9, the pinnacle values of tensile stress within the steel reinforcement at the affected area vary among the slab configurations, with Model N exhibiting the highest stress level at 812.31 MPa. Conversely, the incorporation of studs in Model U15, particularly affixed to the upper-layer bars, yields a decrease in tensile stress, to 763.29 MPa. Similarly, Model B15, featuring studs welded to the lower-layer bars, showcases a further reduction in stress, to 649.67 MPa, thus emphasizing the efficacy of support at the bottom layer. Model UB15, characterized by studs on both upper and lower layers, demonstrates a notable decline in tensile stress, to 631.80 MPa, indicative of the synergistic impact of combined support mechanisms. Similarly, in Models U10, B10, and UB10, the diminished tensile stress levels (756.44 MPa, 722.82 MPa, and 734.15 MPa, respectively) compared to Model N underscore the pivotal role of studs in redistributing and alleviating impact loads. This reduction in stress is ascribed to the enhanced dispersion of loads, the augmented bonding of reinforcement, and the reinforcement of concrete facilitated by the studs, collectively enhancing the structural robustness and resistance to contact-explosion loading of the slabs. Finally, it is noteworthy of mention that the stresses observed in the concrete of the slabs with studs follow a similar trend as observed in the deformations, as shown in Figures 10 and 11. Furthermore, the stresses detected in the concrete correlate with the computed damage pattern.

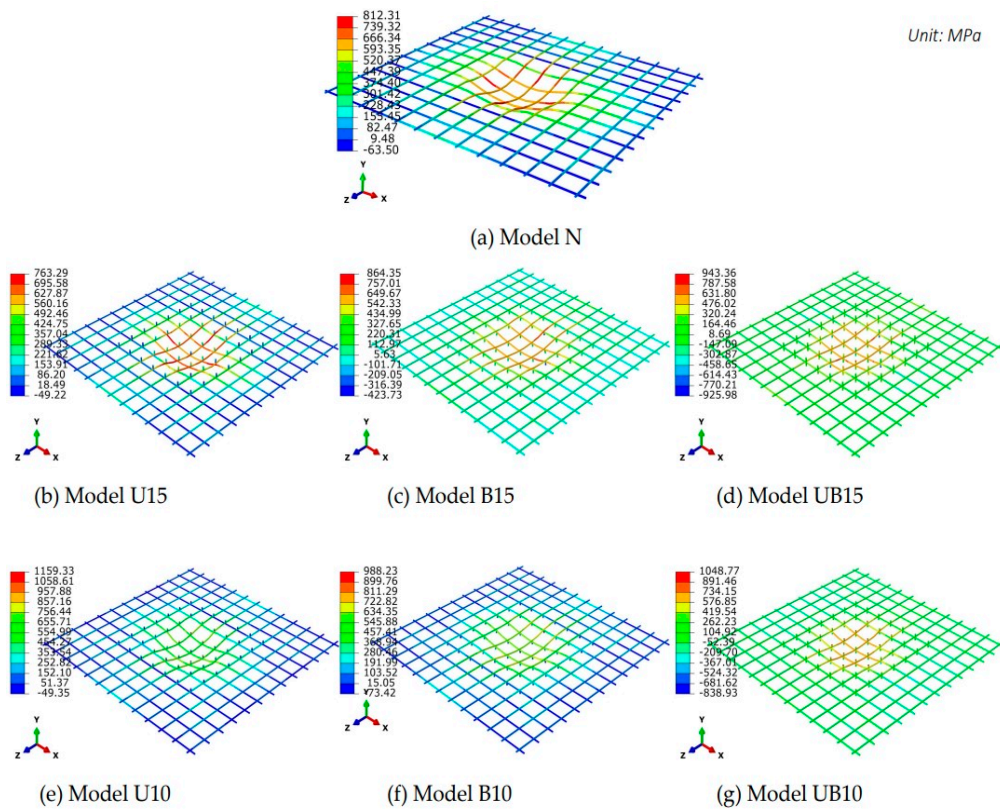


Figure 9. Stresses in the reinforcements of the slabs at $t = 2$ ms.

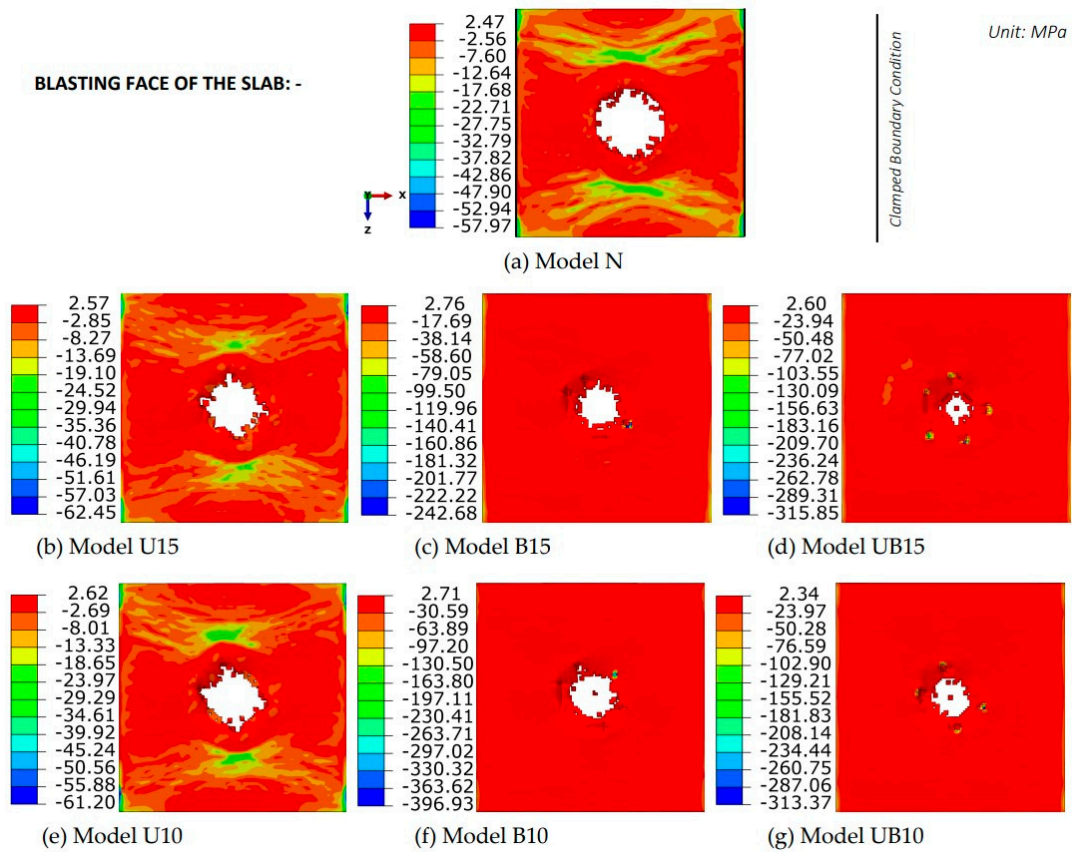


Figure 10. Stresses in the concrete at $t = 2$ ms: Part I.

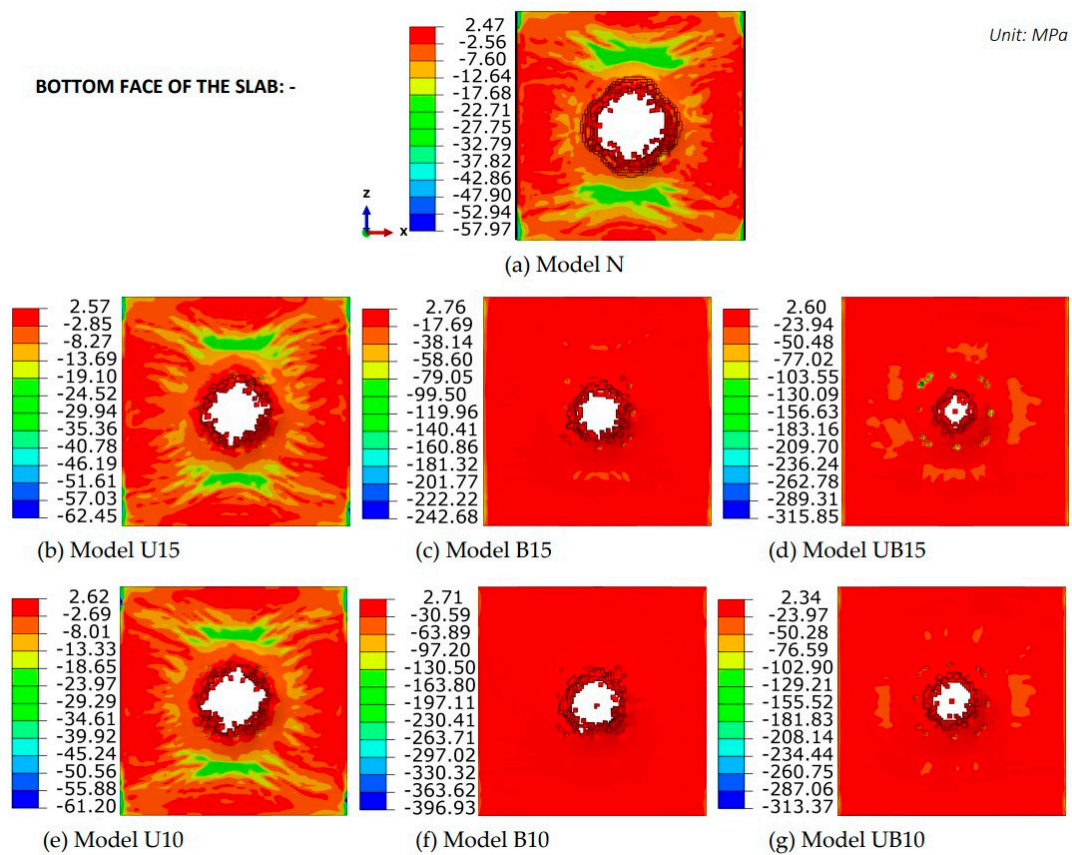


Figure 11. Stresses in the concrete at $t = 2$ ms: Part II.

In Figure 12, in Model N, the absence of studs results in a progressive increase in plastic strain within the concrete over time, culminating in maximal deformation induced by the contact explosion. Perforation begins relatively early, commencing at around 20 microseconds, and swiftly advances, causing extensive damage characterized by sizable perforations. Conversely, in Model U15, where studs are affixed to the upper-layer bars, the evolution of plastic strain follows a similar trajectory, albeit with marginally reduced deformation attributed to the supplementary reinforcement offered by the studs. Perforation onset is delayed, occurring at approximately 60 microseconds, indicative of a postponed structural failure facilitated by the presence of studs, thereby resulting in diminished perforation sizes compared to Model N. Conversely, in Model B15, featuring studs solely on the bottom-layer bars, the escalation of plastic strain transpires more gradually, reflecting the enhanced load distribution and support provided by the bottom-layer studs. Perforation initiates at 1 s, illustrating the efficacy of the bottom-layer studs in retarding structural failure and mitigating the extent of damage. Meanwhile, in Model UB15, equipped with studs on both upper and bottom layers, the evolution of plastic strain exhibits a further reduction in deformation and postponement of perforation onset. Perforation emerges at 1.5 s, substantially later than in Models N and U15, underscoring the augmented resistance to deformation and structural integrity conferred by the combined reinforcement from both layers of studs. Similar patterns are discernible in Models U10, B10, and UB10, where the height of the studs influences the degree of deformation and reduction in perforation size. In summary, the integration of studs, particularly on both upper and bottom layers, fortifies the slab's resilience against deformation and perforation, thereby enhancing its resistance to contact-induced explosions.

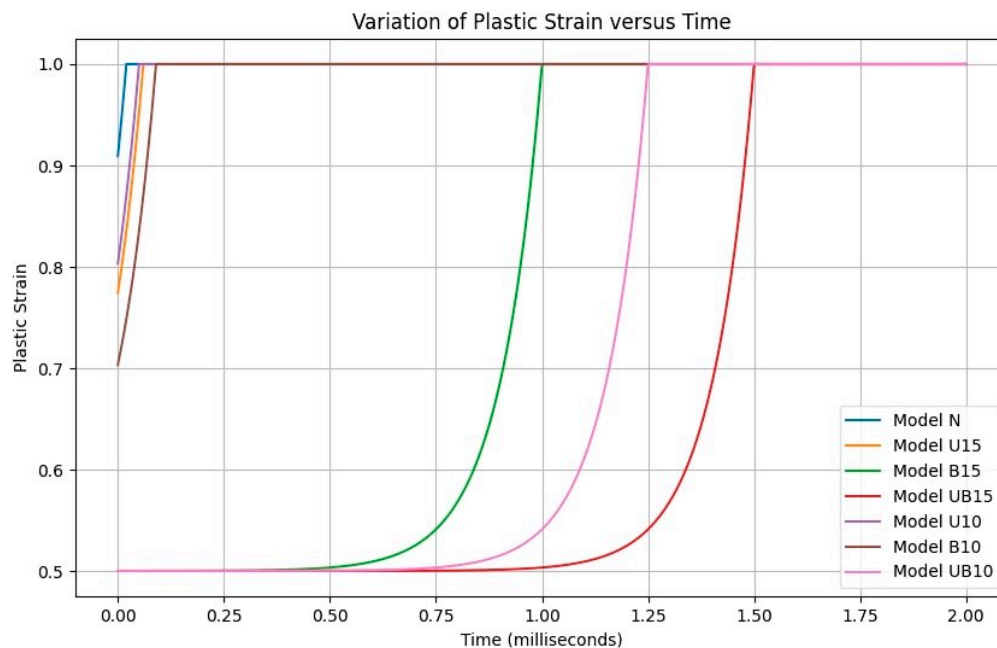


Figure 12. Temporal evolution of plastic strain within the concrete of the slabs at the impacted zone.

Typical damage evident in the slabs comprises spalling on the upper surface, scabbing on the underside, perforations within the blast-affected area, concrete crushing surrounding the perforations, and cracks originating from the perimeter of the perforated zones and extending towards the supporting edges of the slabs, as shown in Figures 13 and 14. The density of cracks on the lower surface of the slab exceeds that on the upper surface due to the slab's inadequate tensile strength. Nonetheless, the integration of studs within the slabs notably diminishes the crack density.

The maximal dimensions of perforations present on the upper and lower surfaces of the slab models undergo significant diminishment with the integration of studs. In the absence of studs, as seen in Model N, these perforation dimensions reach their zenith, measuring $\times 355$ and $z 295$ at the upper surface and $\times 410$ and $z 395$ at the lower surface, indicative of pronounced impairment, as shown in Figures 13–15. Here, “x” denotes the dimension aligned with the unconfined edge of the slab, while “z” denotes the dimension aligned with the restrained edge. Conversely, in Models U15, B15, UB15, U10, B10, and UB10, wherein studs are introduced, there is a marked decrease in perforation sizes. For instance, in Model U15, perforation dimensions are $\times 320$ and $z 280$ at the upper surface and $\times 370$ and $z 295$ at the lower surface, representing a considerable reduction compared to Model N. Similarly, in Model B15, the perforation dimensions decrease to $\times 185$ and $z 225$ at the upper surface and $\times 330$ and $z 235$ at the lower surface, showcasing the efficacy of bottom-layer studs in diminishing damage. Moreover, in Model UB15, the dimensions decrease further, to $\times 160$ and $z 165$ at the upper surface and $\times 200$ and $z 205$ at the lower surface, emphasizing the combined reinforcement provided by studs on both upper and lower layers. Analogous trends are observed in Models U10, B10, and UB10, where variations in stud height influence the degree of reduction in perforation size. This decrease is attributed to the augmented load dispersion, reinforcement, and amelioration of explosion forces afforded by the studs, ultimately bolstering the anti-contact capabilities of the slabs under explosive contact loading. Furthermore, the inclusion of studs alters the damage mechanism from flexure-shear, as observed in Model N, to a prevalent flexure-only mode with diminished cracking, thereby augmenting the structural integrity of the slabs.

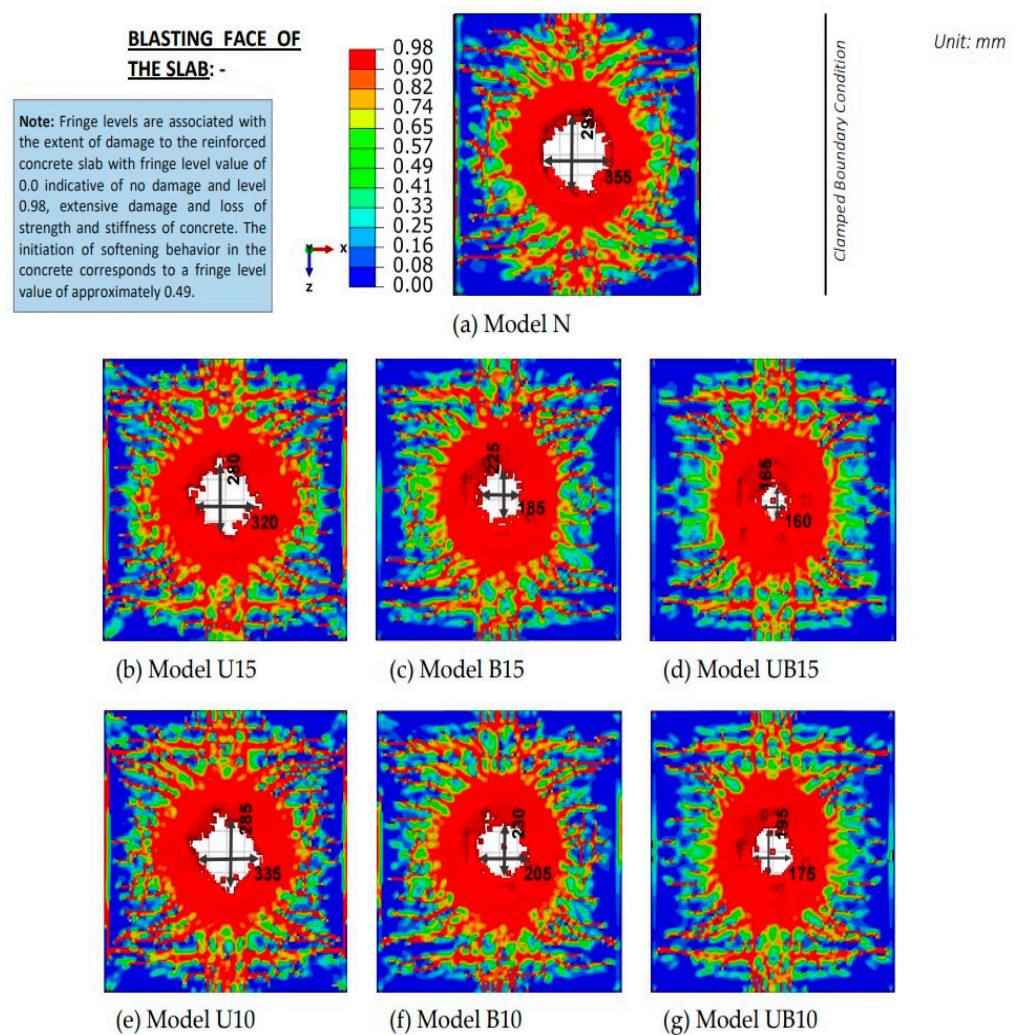


Figure 13. Slab damage: Part I.

The exceptional efficacy of Model UB15 can be ascribed to the synergistic interplay of studs welded with both the upper and lower layers. This arrangement amplifies load dispersion and fortification across the slab, adeptly dispersing blasting forces. Through dual-sided support, the studs within Model UB15 exhibit superior resistance to deformation and deferment of perforation onset. Furthermore, the augmented adherence between concrete and reinforcement diminishes the prospect of detachment or fragmentation. Consequently, Model UB15 manifests diminished perforation dimensions and mitigated structural impairment relative to its counterparts, thereby exemplifying its heightened resilience against touch-off explosions.

Plastic Dissipation Energy (PDE) serves as a pivotal metric within this context, encapsulating the magnitude of plastic deformation endured by the material during explosion events, measured in Joules. In the realm of structural analysis, PDE emerges as a pertinent indicator of damage, offering a quantifiable measure of the material's resilience under stress. Its inclusion in this study provides a nuanced understanding of the structural performance of various models, elucidating the effectiveness of stud incorporation in mitigating blast damage.

Model N demonstrates a PDE of 43.55 J, indicating relatively higher plastic dissipation energy compared to other models. This observation suggests a lesser degree of structural reinforcement within Model N, rendering it more susceptible to deformation and damage under blast loading conditions.

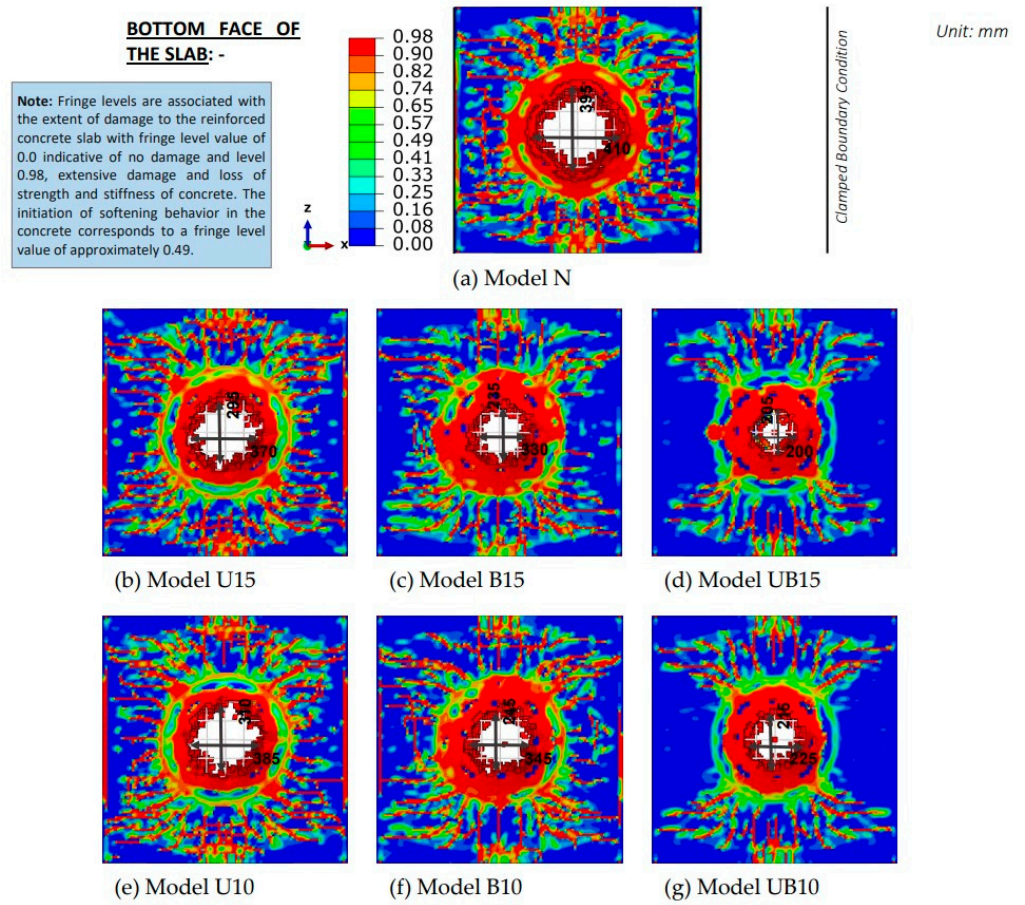


Figure 14. Slab damage: Part II.

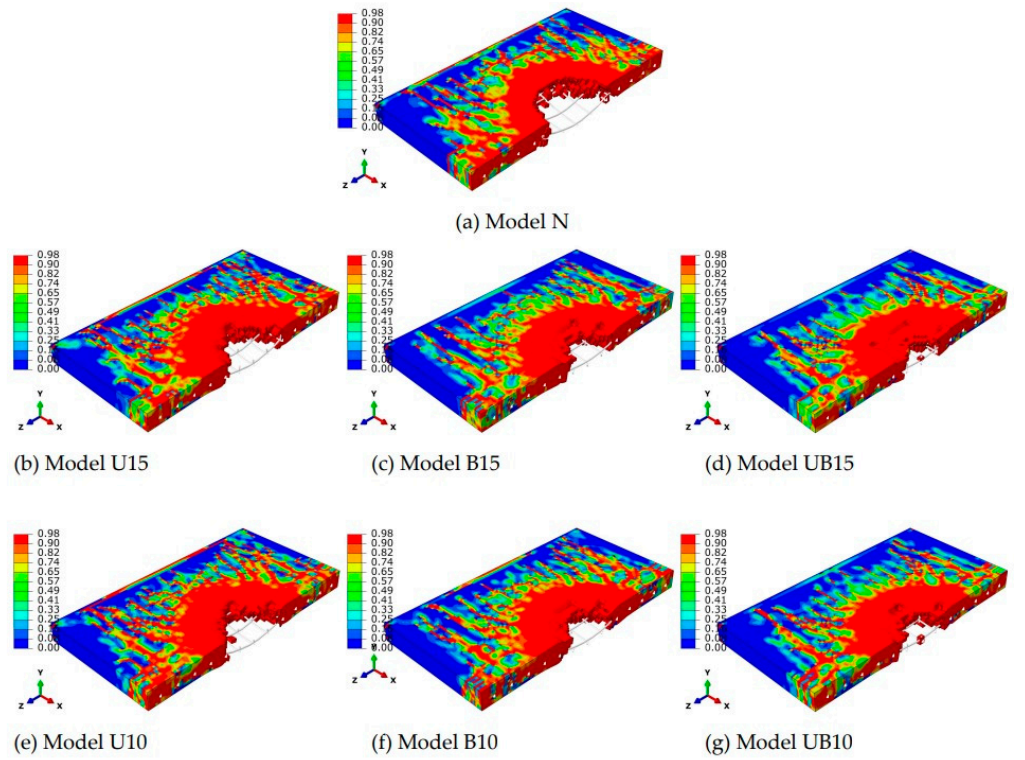


Figure 15. Slab damage: Part III.

Conversely, Model U15 exhibits a PDE of 39.29 J, while Model B15 records a PDE of 22.61 J. Notably, Model UB15 showcases the lowest PDE among the models examined, registering at 19.51 J. This notable reduction in PDE underscores the efficacy of stud incorporation within the slab configuration. The studs serve to enhance load distribution and reinforcement, effectively dispersing explosive forces and minimizing plastic deformation. Moreover, the improved bond between concrete and reinforcement further fortifies the structure, diminishing the likelihood of fragmentation or separation. Furthermore, Model U10 displays a PDE of 40.93 J, and Model B10 presents a PDE of 25.21 J. Lastly, Model UB10 demonstrates a PDE of 21.33 J.

By providing support from both upper and lower layers of re-bars, the studs mitigate deformation and delay the onset of perforation. This dual-sided reinforcement mechanism ensures enhanced resistance to explosive forces, resulting in diminished PDE.

The order of damage severity, based on the ratios of PDE relative to Model N, is as follows:

- (I) Model U10: approximately 93.8%;
- (II) Model U15: $\approx 90.1\%$;
- (III) Model B10: $\approx 57.8\%$;
- (IV) Model B15: $\approx 51.9\%$;
- (V) Model UB10: $\approx 48.9\%$;
- (VI) Model UB15: $\approx 44.8\%$.

This order reflects the models' relative resilience to touch-off explosion, with lower ratios indicating lesser damage severity compared to Model N.

In Figure 16, the graph depicts the correlation between PDE and deformation across multiple models, each distinguished by a unique marker symbol and color. Elevated PDE values correspond to heightened plastic deformation, indicative of increased structural compromise under impact conditions. Notably, Model UB15 showcases the lowest PDE, despite enduring substantial deformation, highlighting its remarkable resilience. This outcome resonates with the technical rationale driving the inclusion of studs in the slab configuration. The incorporation of studs serves to optimize load dispersion, fortify the structural integrity, and defer the onset of perforation, culminating in diminished plastic dissipation energy. As a result, models featuring studs (UB15 and UB10) exhibit superior damage mitigation compared to their studless counterparts (N, U15, B15, U10, and B10), underscoring the efficacy of stud integration in enhancing structural durability against impact loading scenarios.

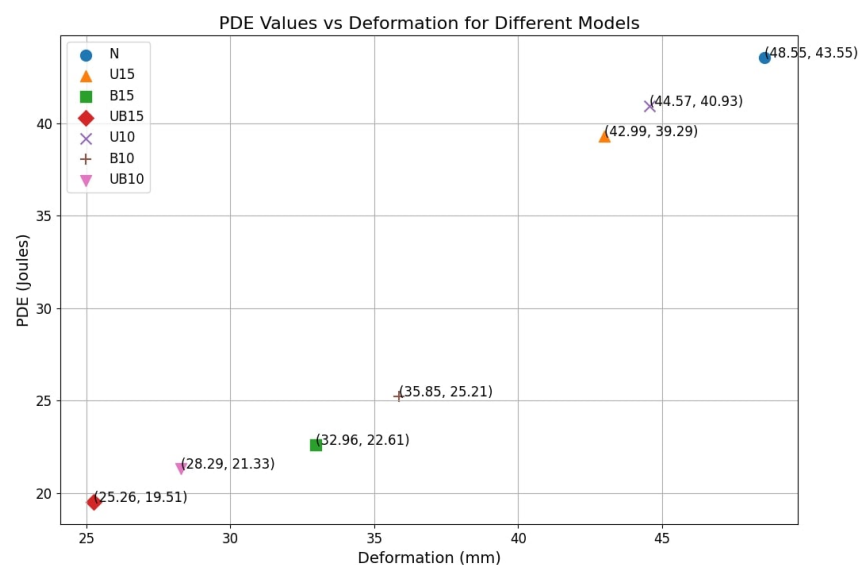


Figure 16. Relationship between PDE and deformation for different slab models.

6. Conclusions and Limitations

In this investigation, the authors delved into the efficacy of integrating studs within concrete slabs to bolster their resilience against detonation-induced loading. By means of computer simulations cross-validated with extant experimental evidence, diverse stud configurations underwent scrutiny to gauge their impact on blast-induced structural damage.

- **Perforation Mitigation:** Perforation stands out as the most prevalent damage incurred during touch-off explosions. Mitigating its severity would constitute a significant advancement, enhancing the structural anti-blast capabilities while concurrently reducing material loss and damages. This endeavor also extends a broader scope for ensuring the safety of building occupants. The present authors have undertaken this investigation by incorporating studs into the slab, eschewing the need for high-strength concrete or bars.
- **Stud Integration Benefits:** the results divulge notable enhancements in blast resistance resulting from stud integration.
- **Effectiveness of Studs:** Both 10 mm and 15 mm studs contribute to load dispersion and reinforcement. Taller studs exhibit heightened effectiveness in attenuating blast-induced structural deterioration.
- **Stud Dimensions' Significance and Impact of Stud Placement:** The pivotal role of stud dimensions as a crucial design parameter for optimizing structural resilience against blast loading scenarios is underscored. Moreover, the study unveiled the intricate interplay between stud placement and the distribution of explosive forces within the slabs.
- **Dual-Sided Stud Reinforcement:** Models featuring studs welded onto both upper and lower layers exhibited superior resistance to deformation and diminished plastic dissipation energy compared to configurations with studs affixed solely to one layer. For instance, Model UB15 showcased the most superior performance, evincing a reduction of approximately 47.91% in deformation and a PDE ratio of approximately 44.8% compared to Model N.
- **Synergistic Effect:** the synergistic effect of dual-sided reinforcement in dispersing blast forces and augmenting structural robustness represents a pioneering advancement in blast-resistant design methodologies.
- **Damage Severity Hierarchy:** Quantitative scrutiny of PDE values delineated the relative resilience of stud-incorporated models. The severity hierarchy of damage, as per PDE ratios, further underscored the efficacy of stud integration, with the order from least- to most-severe damage being as follows: Model UB15, Model UB10, Model B15, Model B10, Model U15, and Model U10.
- **Strategic Stud Placement, Limitations and Considerations:** These findings underscore the significance of strategic stud placement in mitigating blast-induced structural damage. However, it is imperative to acknowledge limitations such as the reliance on computer simulations owing to constraints in experimental testing facilities. Due to factors such as the exorbitant costs, hazards associated with explosions, and the dearth of adequate laboratory resources in academic institutions, computer simulations were utilized as the primary analytical tool. Despite efforts to validate the models with available experimental data, the absence of direct experimental validation may curtail the generalizability of the findings. Additionally, it is noteworthy that while some previous researchers have embraced computer simulations, few have explored live explosion testing and the accompanying challenges, albeit with safety considerations.

A critical constraint of this investigation is the precise positioning of anchoring components (studs), restricted to a central zone measuring 450 mm × 450 mm and maintaining a clearance of 275 mm from all sides of the square slab. This determination is influenced by two primary factors: firstly, the envisioned blast scenario anticipates a touch-off explosion, confining the resultant impacts to a localized area within the explosive region, and secondly, the authors' objective is to mitigate substantial increases in the steel reinforcement ratio

within the slabs. While this focused strategy effectively mitigates blast effects within the designated blast zone, it may not provide optimal reinforcement in scenarios involving blasts occurring away from the central axis. In such scenarios, a more expansive distribution of studs throughout the entire slab would be advisable to ensure comprehensive fortification against potential blast-induced effects across the entirety of the structure. It is noteworthy that in instances of a centrally located touch-off explosion on the slabs, the positioning of studs within a mid-span region has been observed to yield superior effectiveness, as unequivocally evidenced by the findings of the current research endeavor. Consequently, this approach presents a notably more efficient strategy for stud placement.

7. Scope for Future Research

- *Exploration of Alternative Reinforcement Materials:* future studies can explore alternative reinforcement materials beyond traditional studs, such as fiber-reinforced polymers (FRP) or innovative composites, to enhance blast resistance in concrete structures.
- *Optimization of Stud Placement:* further investigations can focus on optimizing stud placement within concrete slabs to maximize blast resilience across different scenarios, utilizing computational techniques or empirical analyses to identify optimal configurations.
- *Experimental Validation:* prioritizing experimental validation of stud integration techniques can enhance the credibility of findings, necessitating strategic investments in experimental infrastructure or collaborative live explosion testing.
- *Impact of Blast Directionality:* analyzing how blast directionality influences stud-integrated concrete slabs' effectiveness in mitigating explosive forces can refine blast-resistant design approaches.
- *Dynamic Behavior of Multi-Story Structures:* extending research to examine the dynamic behavior of multi-story structures with integrated studs offers insights into enhancing blast resilience in complex urban environments.
- *Cost–Benefit Analysis:* conducting thorough cost–benefit analyses comparing stud integration with alternative blast-mitigation strategies informs decision making in construction, highlighting economic feasibility and implementation considerations.
- *Environmental Sustainability:* Investigating the environmental sustainability of stud integration, including its carbon footprint, guides efforts toward eco-friendly infrastructure development practices.

Author Contributions: Conceptualization, S.M.A. and M.A.; methodology, S.M.A. and R.N.A.-D.; software, S.M.A. and R.N.A.-D.; validation, S.M.A., R.N.A.-D., M.S. and M.A.; formal analysis, S.M.A. and M.S.; investigation, S.M.A.; resources, S.M.A.; writing—original draft preparation, S.M.A., M.S. and R.N.A.-D.; writing—review and editing, S.M.A. and M.A.; visualization, M.A.; supervision, M.A.; funding acquisition, R.N.A.-D. All authors have read and agreed to the published version of the manuscript.

Funding: This research received no external funding.

Data Availability Statement: The original contributions presented in the study are included in the article, further inquiries can be directed to the corresponding author.

Conflicts of Interest: The authors declare no conflicts of interest.

References

1. Kyei, C.; Braimah, A. Effects of transverse reinforcement spacing on the response of reinforced concrete columns subjected to blast loading. *Eng. Struct.* **2017**, *142*, 148–164. [[CrossRef](#)]
2. Hao, H.; Hao, Y.; Li, J.; Chen, W. Review of the current practices in blast-resistant analysis and design of concrete structures. *Adv. Struct. Eng.* **2016**, *19*, 1193–1223. [[CrossRef](#)]
3. Zhao, C.; Lu, X.; Wang, Q.; Gautam, A.; Wang, J.; Mo, L.Y. Experimental and numerical investigation of steel-concrete (SC) slabs under contact blast loading. *Eng. Struct.* **2019**, *196*, 109337. [[CrossRef](#)]
4. Thiagarajan, G.; Reynolds, K. Experimental Behavior of High-Strength Concrete One-Way Slabs Subjected to Shock Loading. *ACI Struct. J.* **2017**, *114*, 611–620. [[CrossRef](#)]

5. Anas, S.M.; Shariq, M.; Alam, M.; Umair, M. Evaluation of Critical Damage Location of Contact Blast on Conventionally Reinforced One-way Square Concrete Slab applying CEL-FEM Blast Modeling Technique. *Int. J. Prot. Struct.* **2022**, *13*, 672–715.
6. Li, J.; Hao, H. Numerical study of concrete spall damage due to blast loads. *Int. J. Impact Eng.* **2014**, *68*, 41–55. [[CrossRef](#)]
7. Li, J.; Wu, C.; Hao, H.; Su, Y. Investigation of ultra-high performance concrete under static and blast loads. *Int. J. Prot. Struct.* **2015**, *6*, 217–235. [[CrossRef](#)]
8. Li, J.; Wu, C.; Hao, H. Investigation of ultra-high performance concrete slab and normal strength concrete slab under contact explosion. *Eng. Struct.* **2015**, *102*, 395–408. [[CrossRef](#)]
9. Li, Y.; Chen, Z.; Ren, X.; Tao, R.; Gao, R.; Fang, D. Experimental and numerical study on damage mode of RC slabs under combined blast and fragment loading. *Int. J. Impact Eng.* **2020**, *142*, 103579. [[CrossRef](#)]
10. Lin, X.; Zhang, Y.; Hazell, P.J. Modelling the response of reinforced concrete panels under blast loading. *Mater. Des.* **2014**, *56*, 620–628. [[CrossRef](#)]
11. Schenker, A.; Anteby, I.; Gal, E.; Kivity, Y.; Nizri, E.; Sadot, O.; Michaelis, R.; Levintant, O.; Ben-Dor, G. Full-scale field tests of concrete slabs subjected to blast loads. *Int. J. Impact Eng.* **2008**, *35*, 184–198. [[CrossRef](#)]
12. Shi, S.; Liao, Y.; Peng, X.; Liang, C.; Sun, J. Behavior of polyurea-woven glass fiber mesh composite reinforced RC slabs under contact explosion. *Int. J. Impact Eng.* **2019**, *132*, 103335. [[CrossRef](#)]
13. Thiagarajan, G.; Kadambi, A.V.; Robert, S.; Johnson, C.F. Experimental and finite element analysis of doubly reinforced concrete slabs subjected to blast loads. *Int. J. Impact Eng.* **2015**, *75*, 162–173. [[CrossRef](#)]
14. Wu, C.; Nurwidayati, R.; Oehlers, D.J. Fragmentation from spallation of RC slabs due to airblast loads. *Int. J. Impact Eng.* **2009**, *36*, 1371–1376. [[CrossRef](#)]
15. Wu, C.; Oehlers, D.; Rebentrost, M.; Leach, J.; Whittaker, A. Blast testing of ultra-high performance fibre and FRP-retrofitted concrete slabs. *Eng. Struct.* **2009**, *31*, 2060–2069. [[CrossRef](#)]
16. Abaqus, C.A.E. Damage Plasticity, explicit platform, material library, interactions, constraints, boundary conditions, loads, post-processing. *Help. Learn. Man. Abaqus Ds-Simulia* **2020**.
17. Huff, W.L. *Collapse Strength of a Two-Way-Reinforced Concrete Slab Contained within a Steel Frame Structure*; Final Report; US Army Engineer Waterways Experiment Station: Vicksburg, MI, USA, 1975.
18. Silva, F.P.; Lu, B. Improving the blast resistance capacity of RC slabs with innovative composite materials. *Compos. Part B Eng.* **2007**, *38*, 523–534. [[CrossRef](#)]
19. Lan, S.; Lok, T.-S.; Heng, L. Composite structural panels subjected to explosive loading. *Constr. Build. Mater.* **2005**, *19*, 387–395. [[CrossRef](#)]
20. Zhou, Q.X.; Kuznetsov, A.V.; Hao, H.; Waschl, J. Numerical prediction of concrete slab response to blast loading. *Int. J. Impact Eng.* **2008**, *35*, 1186–1200. [[CrossRef](#)]
21. Tanapornraweekit, G.; Haritos, N.; Mendis, P.; Ngo, T. Modelling of a reinforced concrete panel subjected to blast load by explicit non-linear finite element code. In Proceedings of the Earthquake Engineering in Australia Conference, Wollongong, NSW, Australian, 23 November 2007.
22. Silva, F.P.; Lu, B. Blast resistance capacity of reinforced concrete slabs. *J. Struct. Eng.* **2009**, *135*. [[CrossRef](#)]
23. Du, H.; Li, Z. Numerical analysis of dynamic behavior of RC slabs under blast loading. *Trans. Tianjin Univ.* **2008**, *15*, 61–64. [[CrossRef](#)]
24. Ohkubo, K.; Beppu, M.; Ohno, T.; Satoh, K. Experimental study on the effectiveness of fiber sheet reinforcement on the explosive-resistant performance of concrete plates. *Int. J. Impact Eng.* **2008**, *35*, 1702–1708. [[CrossRef](#)]
25. Zhou, X.Q.; Hao, H. Mesoscale modelling and analysis of damage and fragmentation of concrete slab under contact detonation. *Int. J. Impact Eng.* **2009**, *36*, 1315–1326. [[CrossRef](#)]
26. Morales-Alonso, G.; Cendón, D.A.; Gálvez, F.; Erice, B.; Sánchez-Gálvez, V. Blast response analysis of reinforced concrete slabs: Experimental procedure and numerical simulation. *Trans. ASME J. Appl. Mech.* **2011**, *78*, 051010. [[CrossRef](#)]
27. Zhao, F.C.; Chen, Y.J. Damage mechanism and mode of square reinforced concrete slab subjected to blast loading. *Theor. Appl. Fract. Mech.* **2013**, *63–64*, 54–62. [[CrossRef](#)]
28. Wang, W.; Zhang, D.; Lu, F.; Wang, S.-C.; Tang, F. Experimental study on scaling the explosion resistance of a one-way square reinforced concrete slab under a close-in blast loading. *Int. J. Impact Eng.* **2012**, *49*, 158–164. [[CrossRef](#)]
29. Zhao, F.C.; Chen, J.Y.; Wang, Y.; Lu, S.J. Damage mechanism and response of reinforced concrete containment structure under internal blast loading. *Theor. Appl. Fract. Mech.* **2012**, *61*, 12–20. [[CrossRef](#)]
30. Wang, W.; Zhang, D.; Lu, F.; Wang, C.S.; Tang, F. Experimental study and numerical simulation of the damage mode of a square reinforced concrete slab under close-in explosion. *Engineering Failure Analysis* **2013**, *27*, 41–51. [[CrossRef](#)]
31. Zhang, D.; Yao, S.; Lu, F.; Chen, X.; Lin, G.; Wang, W.; Lin, Y. Experimental study on scaling of RC beams under close-in blast loading. *Eng. Fail. Anal.* **2013**, *33*, 497–504. [[CrossRef](#)]
32. Castedo, R.; Segarra, P.; Alañon, A.; Lopez, L.; Santos, A.; Sanchidrian, J. Air blast resistance of full-scale slabs with different compositions: Numerical modeling and field validation. *Int. J. Impact Eng.* **2015**, *86*, 145–156. [[CrossRef](#)]
33. Qu, Y.; Li, X.; Kong, X.; Zhang, W.; Wang, X. Numerical simulation on dynamic behavior of reinforced concrete beam with initial cracks subjected to air blast loading. *Eng. Struct.* **2016**, *128*, 96–110. [[CrossRef](#)]
34. Yao, S.; Zhang, D.; Chen, X.; Lu, F.; Wang, W. Experimental and numerical study on the dynamic response of RC slabs under blast loading. *Eng. Fail. Anal.* **2016**, *66*, 120–129. [[CrossRef](#)]

35. Zhao, C.; Wang, Q.; Lu, X.; Wang, J. Numerical study on dynamic behaviors of NRC slabs in containment dome subjected to close-in blast loading. *Thin-Walled Struct.* **2019**, *135*, 269–284. [[CrossRef](#)]
36. Pereira, J.M.; Campos, J.; Lourenço, P.B. Experimental study on masonry infill walls under blast loading. In Proceedings of the 9th International Masonry Conference, Guimarães, Portugal, 7–9 July 2014; pp. 1–9.
37. Lin, F.; Dong, Y.; Kuang, X.; Lu, L. Strain Rate Behavior in Tension of Reinforcing Steels HPB235, HRB335, HRB400, and HRB500. *Materials* **2016**, *9*, 1013. [[CrossRef](#)] [[PubMed](#)]

Disclaimer/Publisher’s Note: The statements, opinions and data contained in all publications are solely those of the individual author(s) and contributor(s) and not of MDPI and/or the editor(s). MDPI and/or the editor(s) disclaim responsibility for any injury to people or property resulting from any ideas, methods, instructions or products referred to in the content.